J. Anat. (1982), **134**, 3, pp. 595–631
Printed in Great Britain

Proceedings of the Anatomical Society of Great Britain and Ireland

DECEMBER 1981

The Annual General Meeting of the Society for the Session 1981/2 was held on 10 and 11 December 1981 at Charing Cross Hospital Medical School, London. The Meeting included a Symposium on 'Modern Aspects of Medical Imaging'. The following are authors' abstracts of communications and demonstrations.

1. Experimental model for studying degeneration in unmyelinated fibres. By C. L. CRAWFORD and P. M. D. HARDWICKE. Departments of Anatomy, Charing Cross Hospital Medical School, London, and Biology, Brandeis University, Massachusetts, U.S.A.

There are several available animal models for studying Wallerian degeneration and segmental demyelination in peripheral nerves. Agents such as 6-hydroxydopamine cause degeneration in autonomic unmyelinated fibres. However, there are few experimental models for the study of degeneration in somatic unmyelinated fibres.

We injected Dutch Bantam rabbits in the footpad with a suspension of human sural nerve or dorsal roots plus Freund's complete adjuvant. Six months to 4 years later the rabbits were skin-tested in the back with 0·2 ml 1–10 % dilution of suspension of sural nerve or dorsal roots in saline. Several rabbits responded by developing a papule at 5 weeks. Histologically cells were found resembling the epithelioid cells occurring in granulomatous diseases such as leprosy, tuberculosis or sarcoidosis. Electron microscopic studies showed that some of these cells had infiltrated the cutaneous nerves and there was degeneration of unmyelinated fibres. Axons of myelinated fibres remained normal.

The antigen producing this nerve damage does not appear to be a component of myelin. Very high doses of myelin used in skin tests do not produce epithelioid cells. Instead the antigen appears to reside in the low speed 'nuclear' fraction. Membranes may be obtained from the nuclear fraction of dorsal roots by means of a discontinuous sucrose gradient. When skin-tested these produce damage to unmyelinated fibres. Also deoxycholate-extracted material from the nuclear pellet in doses of 1·5 μg produces severe unmyelinated fibre damage on skin testing. The microsomal and mitochondrial subfractions are negative. The antigen may possibly be a protein or glycoprotein of the Schwann cell plasma membrane.

2. Demyelination: a morphological and electrophysiological correlation. By M. N. GHABRIEL*, G. ALLT, L. SEDAL, M. J. G. HARRISON and JENNIFER R. SMALL. *Departments of Anatomy and Reta Lila Weston Institute of Neurological Studies, The Middlesex Hospital Medical School, London and *Department of Anatomy, Charing Cross Hospital Medical School, London*

In clinical neurology the comparison of the amplitude of muscle action potential induced by nerve stimulation above, and below, localised nerve lesions is widely used as a measure of the severity of local demyelination (Kraft, *Practical Electromyography*, ed. Johnson; Williams & Wilkins; Baltimore, 1980). The validity of this commonly utilised assumption has been tested in an experimental model.

Demyelination was induced by a local injection of lysophosphatidyl choline (LPC, 4–5 μl, 1 %) into the rat tibial nerve at the level of the popliteal fossa in 42 rats. In each animal the contralateral nerve served as a control and in 9 animals the tibial nerve was injected with normal saline instead of LPC (Ghabriel & Allt, *Acta neuropathol.* **52**, 1980). After perfusion fixation, the nerves were examined at the site of injection at 6 days by light and electron microscopy. LPC-injected nerves showed variable degrees of demyelination, the extent of which was estimated on a four-point scale by two independent observers using teased nerve fibre preparations and transverse nerve sections. Control nerves, whether from the contralateral limb, or after saline injection, revealed no demyelination.

Electrophysiologically the amplitude of responses was recorded from the small foot muscles during stimulation of the tibial nerve at two sites separated by the lesion: proximally at the

sciatic notch and distally at the ankle, and the two measurements were expressed as a ratio. Recordings were made both before, and up to, 6 days after LPC and saline injections, and also from contralateral nerves. The normal ratio of amplitude ($0{\cdot}81 \pm 0{\cdot}08$) did not change significantly after saline injection or in the contralateral nerves. After LPC injection, due to a fall in the size of the response to proximal stimulation, a mean decrease of $0{\cdot}27 \pm 0{\cdot}21$ occurred in the amplitude ratio. Comparison of the physiological and histological results indicates that while clinical recordings usually provide a reliable indication of the presence of demyelination they do not accurately reflect the severity of demyelination.

3. Autonomic ganglia in the wall of the adult human urinary bladder. By C. J. GILPIN, J. S. DIXON, S. A. THOMPSON and J. A. GOSLING. *Department of Anatomy, University of Manchester*

Whilst it is generally agreed that autonomic ganglia occur around the bladder base, and in the vicinity of the ureterovesical junctions, there is considerable doubt concerning their distribution throughout the remainder of the adult bladder wall. The present study has employed histological and neurohistochemical techniques to determine the arrangement, distribution and morphological characteristics of autonomic ganglia in the dome and lateral walls of the human urinary bladder. Additional data have been provided by electron microscopy. Biopsy specimens of normal human urinary bladders were obtained either trans-urethrally or during open surgical procedures on the bladder wall.

Ganglia containing 1–20 neurons were consistently observed in the adventitia, within the muscularis and in submucosal locations in specimens obtained from both the dome and lateral walls. Histochemical evaluation of these ganglia revealed intense acetylcholinesterase activity in all nerve cell bodies and their associated pericellular networks of nerve fibres. Neurons and nerve fibres containing catecholamines were never observed in relation to these intramural ganglia. Using the electron microscope numerous presumptive axosomatic synapses were encountered in which the axon terminals contained small (50 nm diameter) agranular and large (100 nm diameter) granulated vesicles.

The morphological findings were discussed in relation to various functional aspects of the human urinary bladder. In addition the clinical relevance of the present findings was considered with particular reference to surgical transection and denervation of the urinary bladder.

4. Baroreceptors in the pulmonary trunk of the domestic fowl. By A. A. M. TAHA (introduced by A. S. KING). *Department of Veterinary Anatomy, University of Liverpool* (Fig. 1)

Baroreceptor activity has been recorded from the pulmonary arteries of mammals (Coleridge and Kidd, *J. Physiol.* **150**, 1960), and mechanoreceptor activity has been recorded from the pulmonary artery of birds (Jones, *Comp. Biochem. Physiol.* **28**, 1969). Nerve fibres have been demonstrated by silver techniques in the media and adventitia of the pulmonary arteries in both birds and mammals, but the presence of baroreceptors has not been established electron microscopically.

The pulmonary trunks from 13 normal domestic fowls were fixed by perfusion and immersion in Karnovsky's solution, and processed for electron microscopy. Toluidine blue thick sections revealed faintly stained modified regions (Fig. 1, M) in the media and adventitia. Electron microscopic examination of these regions disclosed various types of axonal endings. The majority were enlarged, irregular in shape, and characterised by many mitochondria, some of which were abnormal (Fig. 1, arrows). The endings were covered partly by Schwann cells and partly by an extensive basal lamina to which fine collagen fibres were attached. A few of the endings were totally bare except for a basal lamina. Since these endings closely resemble ultrastructurally the baroreceptors of the mammalian carotid sinus and aortic arch, they are interpreted as pulmonary baroreceptors.

Other axonal endings in the modified regions contained small (30–50 nm) or large (60–120 nm) dense-cored granular vesicles, and were considered to be aminergic or peptidergic efferent endings. Yet others contained many clear vesicles (30–50 nm), and were interpreted as cholinergic efferent endings. Sometimes the endings with large dense-cored granular vesicles were separated from the baroreceptors by no more than a wide basal lamina, thus suggesting the possibility of modulation of the stimulus threshold of the baroreceptors.

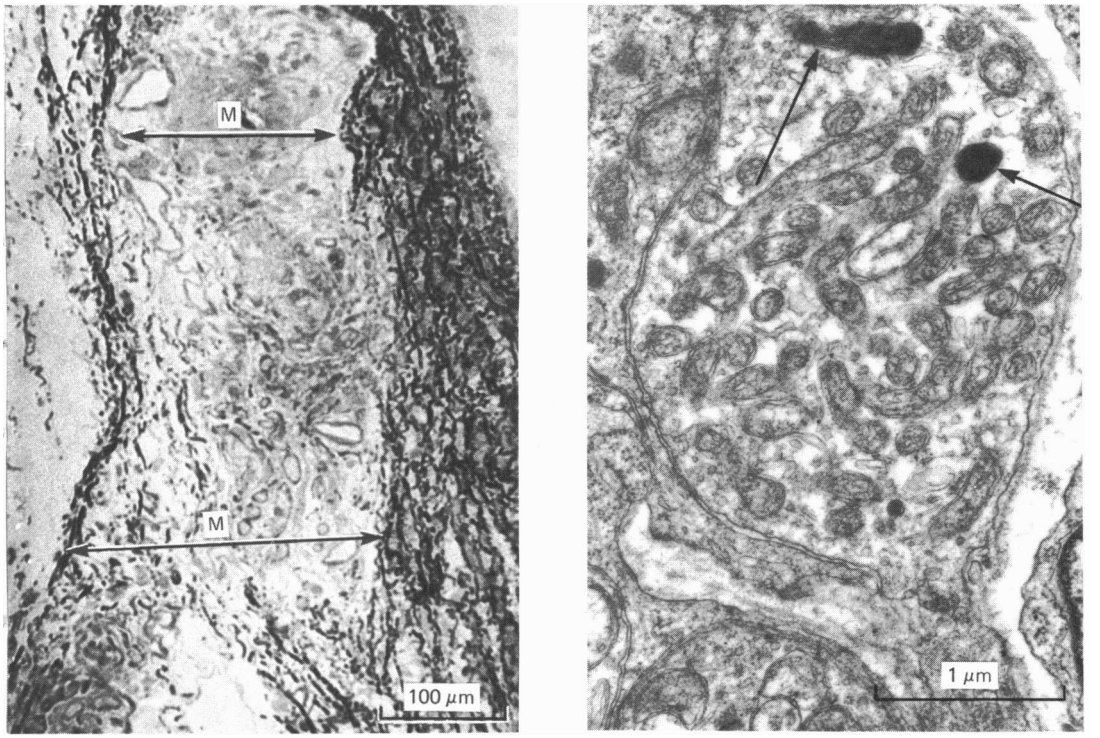

Fig. 1

5. Gliogenesis in the fetal rabbit spinal cord. By R. R. STURROCK. *Department of Anatomy, University of Dundee, Scotland*

Gliogenesis was studied quantitatively in grey matter, and presumptive white matter, in the fetal rabbit spinal cord from E12 to E30. Glia could be identified in the ventral grey matter at E12 and in the ventral and lateral white matter at E14. A rapid increase in the number of glial cells occurred between E20 and E30, especially in white matter.

Counts of mitotic cells indicated that the rapid increase in glial number in white matter was mainly due to division of cells within the white matter, although there was probably also some migration of cells from grey to white matter. Ependymal mitosis contributed little, if anything, to glial production between E20 and E30.

All types of glial cells (oligodendrocytes, astrocytes, microglia and glioblasts) appeared to divide during the rapid phase of gliogenesis. Pyknotic cells were few in number except in the ventral grey matter at E16, when most of the pyknotic cells appeared to be neurons.

There was no evidence at any stage of development of a germinal layer in the spinal cord, similar to the subventricular or subependymal layer which is present in the developing forebrain.

6. Selective neuronal survival in long-term cell cultures of chick embryo spinal cord. By P. L. DEBBAGE. *Department of Anatomy and Embryology, and Centre for Neuroscience, University College London* (Fig. 2)

In cultures of mechanically dissociated central nervous tissue, numbers of neurons survive. They extend processes, are known to form synaptic contacts, and synthesise neurotransmitters. But their survival, in contrast to that reported for explant cultures of similar origin, is typically limited to a few weeks. In cell cultures of chick embryo spinal cord, the majority of well ramified neurons disappear from the cultures during the third and fourth weeks *in vitro*, and there occurs

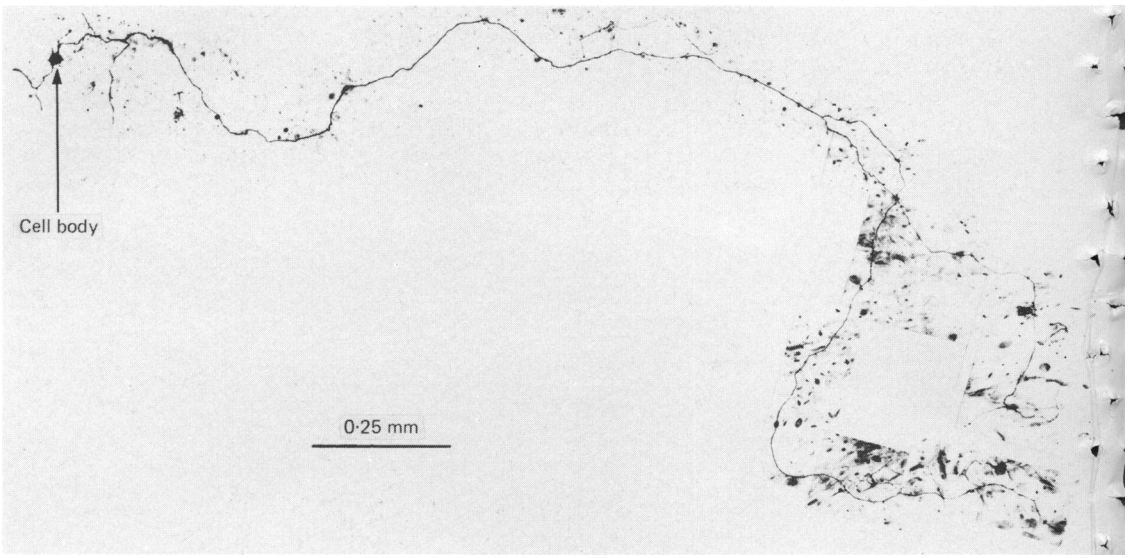

Fig. 2

a concomitant increase in numbers of microglia, which are active phagocytes. Thus older cultures appear to consist of extensive multilayered mats of non-neuronal cells, with a few microglia, and in this condition they can be maintained for many further weeks.

In these older cultures there remains, however, a small number of surviving neurons, representing at maximum no more than 1 % of the neurons originally established in the cultures, and maintaining extensively ramified neurites (Fig. 2) for as long as 16 weeks. They have been seen routinely in many batches of cultures after silver staining and by immunohistochemical demonstration of markers including neurofilament protein (Fig. 2) and synaptosomal membrane components. That these neurons form a single population is suggested by their distinctive form, a major feature of which is that each cell extends at least one fine neurite of great length. Studies in progress aim to demonstrate that these cells share a common origin in the embryonic spinal cord. Their possible identity is considered.

7. Cartographic display of cell migrations into cortical areas of the developing mouse telencephalon.
By I. H. M. SMART. *Department of Anatomy, Medical Sciences Institute, The University, Dundee*

Changes in the depth and nuclear crowding pattern of the intermediate layer were recorded on maps of the developing mouse telencephalon made on each day of prenatal life between E10 and E16. Production of neurons for future cortical areas commenced about E12 in two quite separate locations: one on the medial wall associated with the hippocampus, and one on the lateral wall rostrally producing isocortical neurons. By E14 neuron release had spread from the two original sites over the entire surface of the ventricular layer to form a continuous intermediate layer. During E14 a plate of crowded immature cells (the result of increased neuron release from the periventricular germinal layer) appeared in the outer intermediate layer of the isocortical area and spread over the lateral telencephalic wall passing at E15 over the telencephalic roof into the medial wall. By E16 this type of neuron release had extended as far down the medial wall as the anterior hippocampus, induseum griseum and subiculum which together formed a rostrocaudal band of tissue uninfiltrated by cortical plate. The significance of the cortical plate migration in terms of cell production mechanisms was discussed.

8. A Golgi analysis of the hyperstriatum ventrale in the chick. By P. BRADLEY and G. HORN.* *Department of Anatomy, University of Newcastle upon Tyne and, *Department of Zoology, University of Cambridge* (Fig. 3)

The intermediate and medial parts of the hyperstriatum ventrale (IMHV) of the domestic chick have been implicated in the learning process of imprinting (Horn *et al. Brain Res.* **168**, 1979). The length of the synaptic apposition zones in this region was increased in chicks which had been imprinted (Bradley *et al. Exp. Brain Res.* **41**, 1981). The afferent and efferent con-

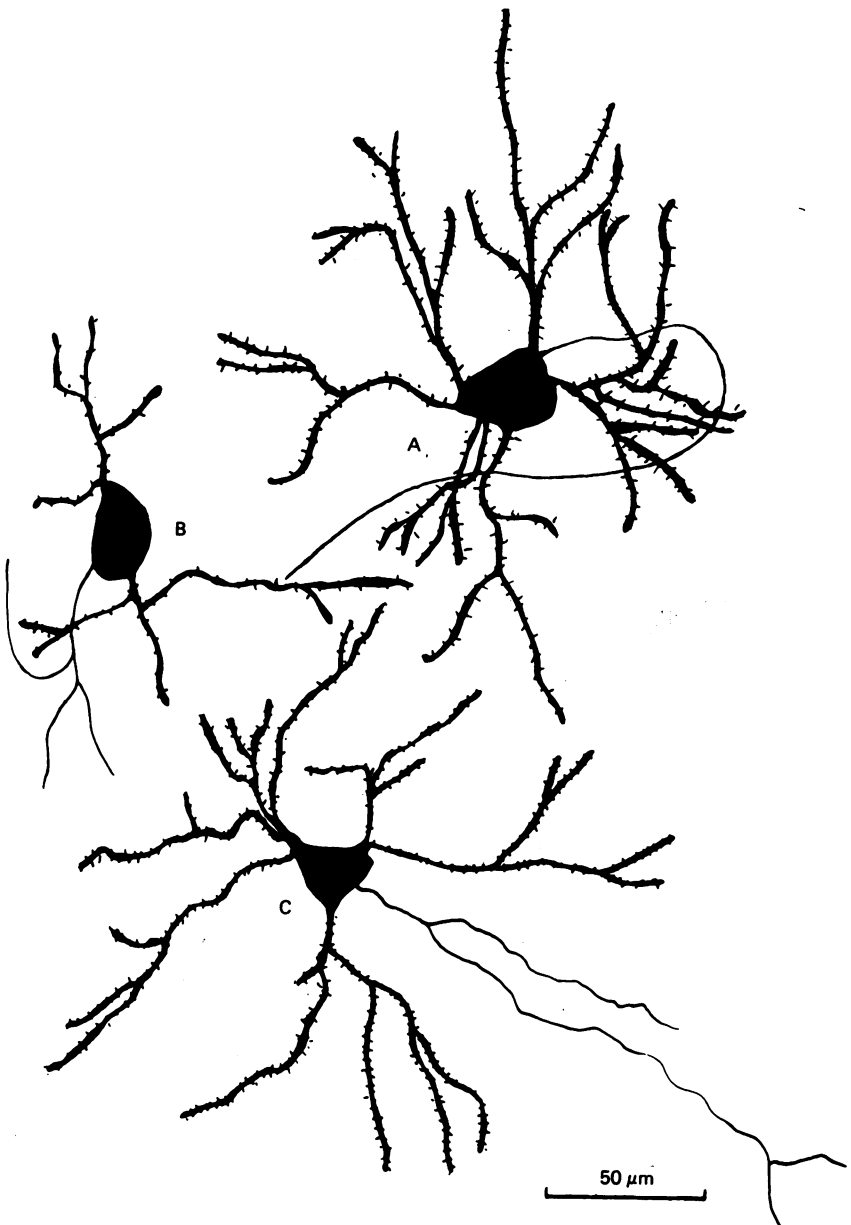

Fig. 3

nections of IHMV have been described (Bradley & Horn, *J. Anat.* **128**, 1979; Bradley & Horn, *J. Physiol.* **278**, 1978; Davies & Bradley, *J. Anat.* **133**, 1981) but the cellular organisation of this region has not previously been studied. We report here the results of a Golgi analysis of the neuronal components of IMHV.

Camera lucida drawings of a total of 140 Golgi-impregnated neurons from the IMHV of ten light-reared Ross 1 chicks 1 day old were analysed. Cells were classified according to size, shape of soma and number of primary dendrites arising from the soma. Fifty six (40 %) of the cells were large multipolar neurons (Fig. 3A). The dendrites of these cells displayed no specific orientation although the dendritic tree was least extensive posteroventrally. The origin and course of the axons of these cells were highly variable. Twenty seven (20 %) of the cells were large pyramid shaped neurons (Fig. 3C) which showed a definite dorsomedial orientation of the apical dendrite. The axons of these cells ran in a direction opposite to that of the apical dendrite and commonly bifurcated in a 'pitchfork' fashion prior to leaving IMHV. Twenty one (15 %) of the cells had large ovoid cell bodies with a maximum of four primary dendrites (Fig. 3B). The axons of these cells divided into a number of branches soon after leaving the cell body. The long axes of these cells tended to be orientated dorsoventrally. The remainder of the cells were classified as small pyramidal or stellate neurons. No specific lamination of the cells was observed.

9. The distribution of acetylcholinesterase in the chick telencephalon. By B. J. McCabe, G. Horn and G. McGrath.* *Department of Zoology, University of Cambridge, and *Department of Anatomy, University of Bristol* (Fig. 4)

Acetylcholinesterase activity in the forebrain hemispheres of the chick changes markedly during development (Marchand *et al. FEBS Lett.* **78**, 1977) and is influenced by visual experience (Haywood *et al. Brain Res.* **92**, 1975). The anatomical distribution of enzyme activity is not known and was investigated in the present study.

Fourteen Ross 1 chicks were anaesthetised 1–2 days post-hatching with sodium thiopentone. Eight birds were anaesthetised 6 weeks after hatching. Brains were fixed by intracardiac perfusion with 20 % formalin in 154 mM-Na_2SO_4 followed by immersion in 10 % neutral formalin

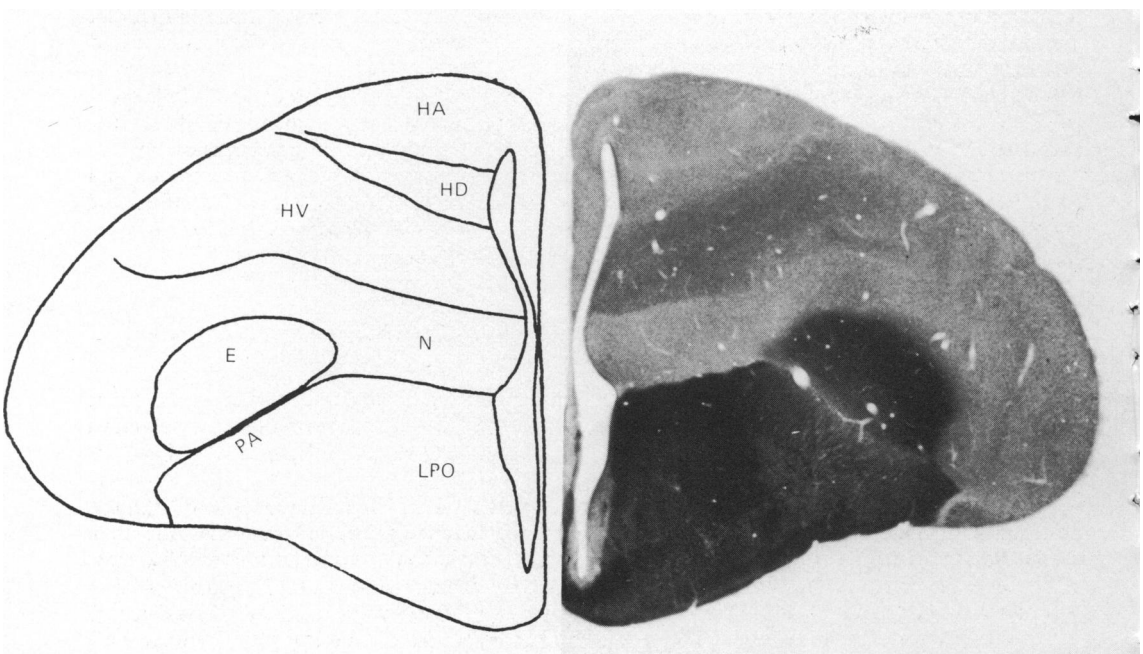

Fig. 4. HA, hyperstriatum accessorium; HD, hyperstriatum dorsale; HV, hyperstriatum ventrale; N, neostriatum; E, ectostriatum; PA, paleostriatum augmentatum; LPO, lobus parolfactorius. Scale × 4.

at 4 °C for 18 h. Frozen sections 60 or 80 μm thick were stained for acetylcholinesterase (Lewis, *Bibliotheca anat.* **2**, 1961). Incubation time was 3–5 h at room temperature (pH 5·6). Sections incubated at the same time with butyrylthiocholine iodide were unstained. Results were confirmed on fresh frozen sections cut from two additional brains from 1 day old chicks.

Stained cell body profiles were observed in hyperstriatum accessorium, hyperstriatum intracalatus/dorsale, neostriatum and the olfactory bulb (particularly the mitral cell layer). In addition to stained cell body profiles, diffuse staining (presumably of neuropil) occurred in hyperstriatum ventrale (in which dorsal and ventral laminae could be distinguished), paleostriatum augmentatum, paleostriatum primitivum, lobus parolfactorius, dorsal archistriatum, septal nuclei, caudal neostriatum and ectostriatum (Fig. 4). Nucleus basalis contained dense diffuse staining. Intensely stained cell bodies and fibres were observed in the nucleus intrapeduncularis.

In chickens aged 6 weeks the overall pattern of staining was similar to that in the 1–2 day old chick.

10. The projection of the somatosensory cortex on the superior colliculus of the rat. By H. N. RAMADAN and K. E. WEBSTER. *Department of Anatomy, King's College London*

The ascending somatosensory input to the intermediate and deep layers of the rat superior colliculus is organised to produce a body map congruent with the visual field (Webster & Ramadan, *J. Anat.* **133**, 1981). A second source of somatic information to the colliculus is the somatosensory cortex. We have examined the organisation of this system by using the Fink and Heimer technique after making small cortical lesions; and by exploiting the uptake and transport of [^{3}H]amino acids or horseradish peroxidase (HRP) injected into cortex or colliculus (Ramadan & Webster, *J. Anat.* **133**, 1981).

The Fink and Heimer and autoradiographic material shows the corticotectal axons to arise from perikarya deep to layer IV of the ipsilateral somatosensory cortex, and to end in the intermediate and deep layers of the colliculus, which the axons enter from its rostral and lateral borders. Like those from the spinotectal tract (Antonetty & Webster, *J. comp. Neurol.* **163**, 1975), the terminals aggregate into clusters separated by relatively empty areas. It is therefore possible that the two inputs interdigitate rather than converge. Axons from medial cortex (tail and hindlimb – Welker, *J. comp. Neurol.* **166** 1976) end in the caudal and medial colliculus; those from face areas distribute laterally and rostrally; those from intermediate cortex end between those two zones.

The HRP studies confirm that the descending projection arises from pyramidal cells in layer V of the ipsilateral primary and secondary somatosensory cortices. Although its significance is dismissed by Wise & Jones (*Brain Res.* **133**, 1977), the mode of entry to the colliculus of corticotectal axons makes inevitable the uptake of HRP by axons of passage in all but extremely caudal or medial injections. Only when due allowance is made for this is it possible to confirm the mapping described above. The 'descending' somatic map occupies the same collicular layer as, and is congruent with, the map derived from ascending projections.

11. The combined effects of nutrition and environmental diversity on body and brain growth in rats. By P. G. BHIDE and K. S. BEDI. *Department of Anatomy, University of Aberdeen*

Both undernutrition and environmental enrichment during early life are known to cause alterations in various brain characteristics. However, there are few reports on the interaction effects of nutrition and environment on brain structure. This report is based on such an investigation.

Rats were undernourished from the 16th day of gestation to 25 postnatal days of age (by restriction of their mothers' diet to about 50 % of that eaten by well-fed controls) and then weaned on to an *ad libitum* diet. Around 35 days of age, 12 previously undernourished (PU) male pups were assigned to an 'enriched environmental condition' (EC) and 12 to an 'isolated environmental condition' (IC). Well-fed controls were similarly assigned. The EC consisted of 12 rats living together in a large ($48 \times 36 \times 62$ cm^3) metal cage containing 'toys' which were changed daily. The IC animals were singly housed in small ($21 \times 18 \times 33$ cm^3) opaque plastic cages without 'toys'. After 30 days in these conditions all rats were killed by perfusion with 10 % formol saline.

In both the well-fed and previously undernourished groups, the EC rats were significantly lighter ($P < 0{\cdot}01$) than the IC rats. The 'forebrains' of the EC rats were about 4 % heavier ($P < 0{\cdot}03$) than those of the IC. The thicknesses of the occipital cortex, measured on coronal sections at and just behind the level of the posterior commissure, were between 6 % and 10 % greater ($P < 0{\cdot}01$) in the EC rats compared to the IC rats, irrespective of previous nutritional status. The cortex of the frontal lobe region showed no such change. There were no significant interactions between nutrition and environment in any of the features investigated. It appears therefore that environment has an effect almost similar in magnitude and direction in both well-nourished and previously undernourished rat brains.

12. A possible explanation of the synaptic and neuronal deficits and distortions induced by undernutrition during early life. By K. S. BEDI. *Department of Anatomy, University of Aberdeen* (Fig. 5).

Undernutrition of rats during early life causes deficits and distortions of brain structure. Some of these are permanent; others show evidence of 'catch-up', or recovery, in later life. For instance, the cerebellar granule-to-Purkinje cell ratio shows a persisting deficit of about 25 % in rats previously undernourished during early life. On the other hand, the 30–37 % deficit in the cerebellar synapse-to-neuron (S/N) ratio, observed immediately after the period of undernutrition, disappeared in later life (Bedi *et al. J. comp. Neurol.* **193**, 1980*a*, *b*).

In this paper a simple model system offers an explanation of how such changes in the brain may occur. Consider a neuronal population set consisting of three neurons A, B and C in a normal rat brain (Fig. 5*a*). Each neuron is capable of making just two efferent and two afferent synaptic contacts. This gives a S/N ratio of two. Loss of a neuron (say C) either through cell death or failure of development due to undernutrition would also cause the loss of the (potential)

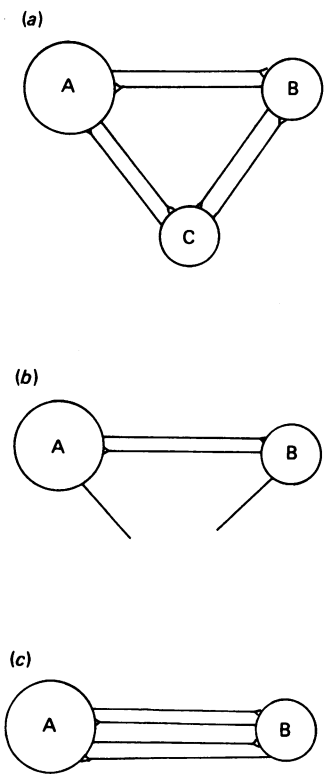

Fig. 5

afferent and efferent synapses associated with that neuron (Fig. 5*b*). This gives a S/N ratio of 1, i.e. a 50% deficit.

Nutritional rehabilitation could allow the dendrites to grow and 'retarget' on to the remaining neurons leading to the formation of 'new' synapses. This would result in two neurons and four synapses restoring the original S/N ratio of 2 (Fig. 5*c*).

Furthermore, if neuron A is of (say) type Z and neurons B and C are of type Y then loss of a single type Y neuron causes a permanent alteration of the ratio between the two types of neuron. Neurogenesis does not occur in adult animals so the original ratio cannot be restored.

In conclusion, the model presented offers an explanation for the observations that undernutrition during early life can cause permanent distortions of the ratios between different types of neuron, but only a temporary alteration in the synapse-to-neuron ratio.

13. A new concept of lung development. By ANK A. W. TEN HAVE-OPBROEK. *Department of Anatomy and Embryology, University of Leiden, The Netherlands.*

The classic model of mammalian lung development (i.e. the division into periods) was tested in the mouse by using recent immunological (Ten Have-Opbroek, *Devl Biol.* **46**, 1975, and **69**, 1979; *Am. J. Anat.*, in the Press), and autoradiographic (Adamson & Bowden, *Lab. Invest.* **30**, 1974; Kauffman *et al. Anat. Rec.* **180**, 1974; Evans *et al. Exp. mol. Pathol.* **22**, 1975) data concerning the nature of the epithelial cells in the lung. This evaluation showed that the model in question is not tenable for the mouse or, very probably, for any other mammal.

On the basis of the recent data, the course of lung development in mammals can be defined as follows (Ten Have-Opbroek, *Am. J. Anat.*, in the Press). The lung primordium gives rise, for each of the prospective lungs, to a system called the primordial system, which consists of tubular structures lined by columnar epithelium (called primordial tubules). This system differentiates into a system consisting of two sharply demarcated parts: a proximal part with columnar epithelium and a distal part with cuboidal epithelium. The former part gives rise to the air-conducting portion of the lung, the latter to the respiratory portion. The components of these parts are called bronchial and acinar tubules respectively.

The acinar tubule is the basic structure in the genesis of the respiratory unit or acinus pulmonaris. Its lining is composed of great alveolar (= type II) cells, or their precursor cells. Pre- and postnatally, the acinar tubule gives rise to tubular, saccular, and pouch-like derivative structures. Besides the great alveolar cell (or precursor), their lining contains the small alveolar (= type I) cell (or precursor) that originates from the former. These derivative structures together constitute the definite acinus pulmonaris. In the latter, the structures occurring in the adult lung can be discerned, i.e. the respiratory bronchiole, the alveolar duct, and the alveolar sac.

14. Development of the guinea-pig lung between the pseudoglandular and canalicular stages. By A. PRENTICE and R. J. SCOTHORNE. *Department of Anatomy, University of Glasgow*

In the development of the mammalian lung, three stages are now generally recognized: the pseudoglandular, canalicular and terminal sac stages. The transformation between the first two involves elongation and expansion of the future respiratory division of the airway, thinning of its epithelial lining and a closer association between its epithelium and the capillary plexuses. These changes collectively lead to the initial establishment of the future blood–air barrier. This paper re-examines these events in the guinea-pig lung, by morphometric analysis of semithin plastic sections, from three groups, each of three animals, at 39, 46 and 52 days of gestation, using the MOP electronic planimeter. Measurements were made of five subpleural areas from each animal, and the results for each stage were pooled.

Table 1 shows the mean percentage contribution of each of the major constituents – microvasculature, airway (= air space and airway epithelium) and mesenchyme – at the pseudoglandular and canalicular stages and at a stage transitional between the two.

These figures show (i) a very large increase in the relative volume of the future 'air space' ($P < 0{\cdot}01$), (ii) a reduction in the mesenchyme, between pseudoglandular and transitional stages ($P < 0{\cdot}01$) and (iii) an insignificant increase in the relative volume of microvasculature.

Table 1

Stage	Microvasculature (V_{cap})	Airway (V_a) Airspace V_s	Airway (V_a) Epithelium V_e	Mesenchyme (V_m)
Pseudoglandular	13 %	4 %	27 %	56 %
'Transitional'	13 %	13 %	28 %	46 %
Canalicular	15 %	28 %	57 %*	

* The respiratory epithelium is included in 'mesenchyme' because it was too thin to be separately resolved by optical microscopy.

Table 2 shows the total surface area, per unit volume, of microvasculature and of future air space at the three stages. These figures show (i) a 4-fold increase in surface area of the air space and (ii) a 1·7-fold increase in surface area of the microvasculature ($P < 0{\cdot}01$). This correlates with the replacement of sinusoidal vessels by a larger number of capillaries of smaller mean diameter, but having the same total relative volume (cf. Table 1).

Table 2

Stage	Microvasculature (S_v)	Airspace (S_a)
Pseudoglandular	0·0602	0·0142
'Transitional'	0·0742	0·0304
Canalicular	0·1057	0·0584

These findings, together with the histological appearances, lead us to question the current consensus that there is greatly increased vascularisation of the lung, and that the capillaries are the active agent in thinning of the respiratory epithelium, during the transformation.

15. A morphometric comparison of the lungs of two species of bird of different exercise capacities. By J. N. MAINA (introduced by A. S. KING). *Department of Veterinary Anatomy, University of Liverpool*

Structural–functional correlations in the design of the mammalian lungs for gaseous exchange are now well established (Gehr *et al. Respir. Physiol.* **44**, 1981). The present lack of comprehensive quantitative data on the structure of the avian lung does not enable such a correlation to be attempted in birds, and makes comparison with mammals and other vertebrates unsatisfactory. Therefore a comparative morphometric investigation has been made of the gas exchange apparatus in the domestic fowl (*Gallus domesticus*), an inactive bird, and in the wild mallard (*Anas platyrhynchos*), a powerful flyer.

The birds were killed by an intravenous injection of barbiturate and weighed. The lungs were fixed *in situ* by tracheal perfusion with buffered 2·3 % glutaraldehyde. Lung volumes were determined by a water displacement method. For each bird the left and right lungs were sampled by a stratified procedure for light and electron microscopy respectively, and processed by standard techniques. Histological sections were analysed by point-counting to determine the volume densities of the main functional components of the lung, notably the exchange tissue; absolute volumes were calculated from the lung volume.

From ultrathin resin sections a sufficient number of electron micrographs was analysed using a quadratic lattice grid by standard morphometric methods (Weibel, *Respir. Physiol.* **11**, 1970/1). The results are expressed as means (± S.D.) and appertain to the left and right lungs together (Table 1).

Table 1

N =	*Gallus* 5	*Anas* 5
Weight (kg)	2·06 ± 0·58	1·04 ± 0·09
Vol. lungs (cm^3)	25·00 ± 2·60	30·39 ± 3·74
S_A of b-g.b. (m^2)*	2·08 ± 0·09	2·97 ± 0·54
S_A of b-g.b./g. body weight (cm^2/g)	10·10 ± 0·95	28·60 ± 2·71
S_A of b-g.b./vol. of exchange tissue (mm^2/mm^3)	180·00 ± 8·80	241·00 ± 14·21
Capillary loading (cm^3/m^2)	1·69 ± 0·11	1·37 ± 0·09
Harmonic mean thickness		
b-g.b. (μm)	0·31 ± 0·02	0·13 ± 0·01
Plasma (μm)	0·34 ± 0·05	0·37 ± 0·03
Arithmetic mean thickness: b-g.b. (μm)	1·20 ± 0·06	0·90 ± 0·13

* S_A, surface area; b-g.b., blood–gas barrier.

This morphometric comparison of the lungs of these two species of birds points to a substantial superiority in *Anas* in the anatomical adaptations of its lungs for gas exchange, in response to its much more energetic mode of life.

16. Coelomic cavity formation in the early chick embryo: some morphological aspects as seen with the scanning electron microscope (SEM). By C. N. B. TAGOE. *Department of Anatomy, Leicester University Medical School* (Fig. 6).

During its formation the chick embryo mesoderm changes from a monolayer to a multilayer of different thicknesses; this particular modification occurs between Hamburger and Hamilton stages 3 and 5 and has been noted with the SEM (England & Wakely, 1977). Subsequent morphological changes in the lateral plate mesoderm, prior to and during the formation of the coelomic cavity, are reported here.

At stage 6 the lateral plate mesoderm cells form a bilaminar sheet and are closely packed together with only small intercellular spaces between them. They are attached to each other, and to adjacent ectoderm and endoderm, by means of fine processes. Their general shape is columnar (Fig. 6A). The above pattern is seen consistently in sections along the planes (*a*, *b*, *c*) shown in Fig. 6B.

At stage 7 when the coelom begins to appear, the cells of the somatic mesoderm flatten out (Fig. 6C). The flattening out is also seen on examining the luminal surface of the somatic mesoderm. A cobblestone pattern is seen on the luminal surface of the splanchnic mesoderm.

Both luminal surfaces possess variable amounts of short processes but are completely devoid of extracellular material, as seen by SEM.

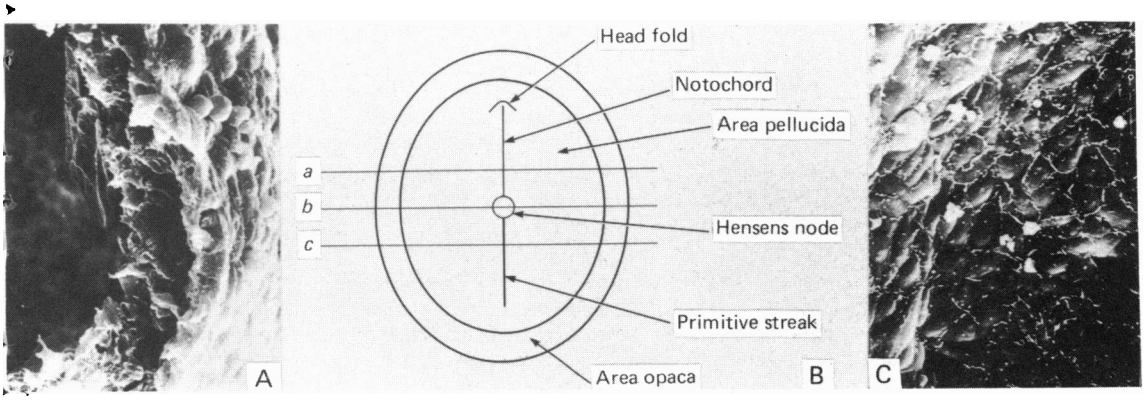

Fig. 6

The changes described take place in a cephalocaudal direction, and also from the periphery towards the midline. This results in a horseshoe pattern of morphological changes, with a gap cephalad in the region of the proamnion.

That the lateral plate mesoderm cells are rearranged into two definite layers at stage 6 is significant, because it is from this stage onwards that the coelom begins to form between these two layers. It is not immediately clear why somatic mesoderm cells flatten out while those of the splanchnic mesoderm remain columnar.

17. Localisation of the sodium pump in the epiblast of the early chick embryo. By C. D. STERN (introduced by P. L. DEBBAGE). *Department of Anatomy and Embryology, University College London* (Fig. 7).

Previous electrophysiological studies (Jaffe & Stern, *Science* **206**, 1979) have shown that strong electrical currents flow out of the primitive streak of chick embryos during gastrulation. They are probably the result of ion pumping by the epiblast into the underlying intrablastodermic space. Sodium is likely to be the current-carrying ion (Howard, *J. cell. comp. Physiol.* **50**, 1957). These studies have led me to investigate the localisation of the sodium pump in the epiblast of the early chick embryo by exposing early, middle and late gastrula blastoderms to tritiated ouabain, which binds specifically to the sodium/potassium pump.

Each of the embryos was exposed to 6 μCi tritiated ouabain in saline/albumen (1:1) (final ouabain concentration, 2×10^{-7} M, specific activity, 17 Ci/mmol) for 30 min at 37 °C. The embryos were grown on their vitelline membranes (New, *J. Embryol. exp. Morph.* **3**, 1955) on a pool of the label-containing medium. The blastoderms were fixed in Bouin's fixative and embedded in paraffin wax, or briefly fixed in buffered formal saline and sectioned in a cryostat after freezing in isopentane cooled with liquid nitrogen. The sections (8–20 μm) were coated with Ilford Nuclear Research Emulsion K 2. The slides were exposed for 4 weeks at 4 °C and developed in Kodak D 19b. The autoradiographs were photographed by dark-field optics.

The results show that prior to the appearance of the primitive streak ouabain binding is

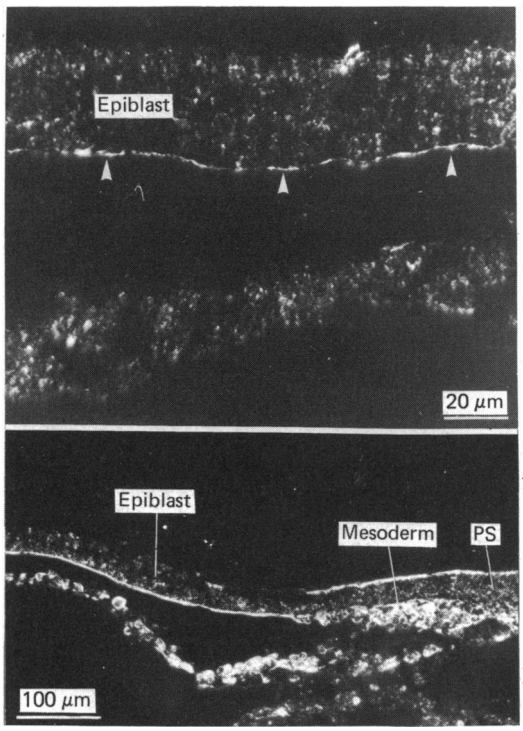

Fig. 7

localised near the basal surfaces of the epiblast cells (Fig. 7, arrowheads). After the emergence of the mesoderm from the streak, the labelling remains at the basal side in lateral regions but it shifts to the apical side of the tissue at the primitive streak (Fig. 7, PS). Both figures are transverse sections through the embryos. Control embryos incubated at 4 °C, or using a medium containing 20 mM potassium, did not show the above localisation.

From these experiments it can be concluded that ouabain binding sites are probably restricted to the basal (ventral) surface of the epiblast cells during gastrulation in the early chick embryo, except at the primitive streak where they appear at the apical (dorsal) surface of the cells. There is thus a close correspondence between the pattern of current flow and the position of the pumps, suggesting that sodium may therefore be the major current-carrying ion.

18. A scanning electron microscopic study of prenatal muscle development *in vivo*. By N. C. STICKLAND. *Department of Anatomy, Royal (Dick) School of Veterinary Studies, Edinburgh* (Fig. 8).

Early stages of myoblast fusion have been studied in tissue culture preparations and some of these studies have employed scanning electron microscopy. Structural aspects of muscle development *in vivo*, however, have been studied almost exclusively using sectioning techniques. Theories of muscle development, based on these latter studies, include deductions about the longitudinal arrangement of cells and fibres in developing muscle. Scanning electron microscopy of muscle tissue *in vivo* provides a method whereby our knowledge of the three dimensional arrangement of developing muscle may be extended.

Mouse fetuses (C57 strain) were obtained at daily intervals from 12 days gestation to almost full term (18 days). Whole forelimbs were dissected off the fetuses and fixed in 3 % glutaraldehyde. In the older fetuses (> 15 days) m. biceps brachii was then removed entirely whereas in the younger fetuses the muscle was left *in situ*. The muscles were pulled apart to expose the developing muscle fibres and then processed and critical point dried. Freeze-drying techniques were also

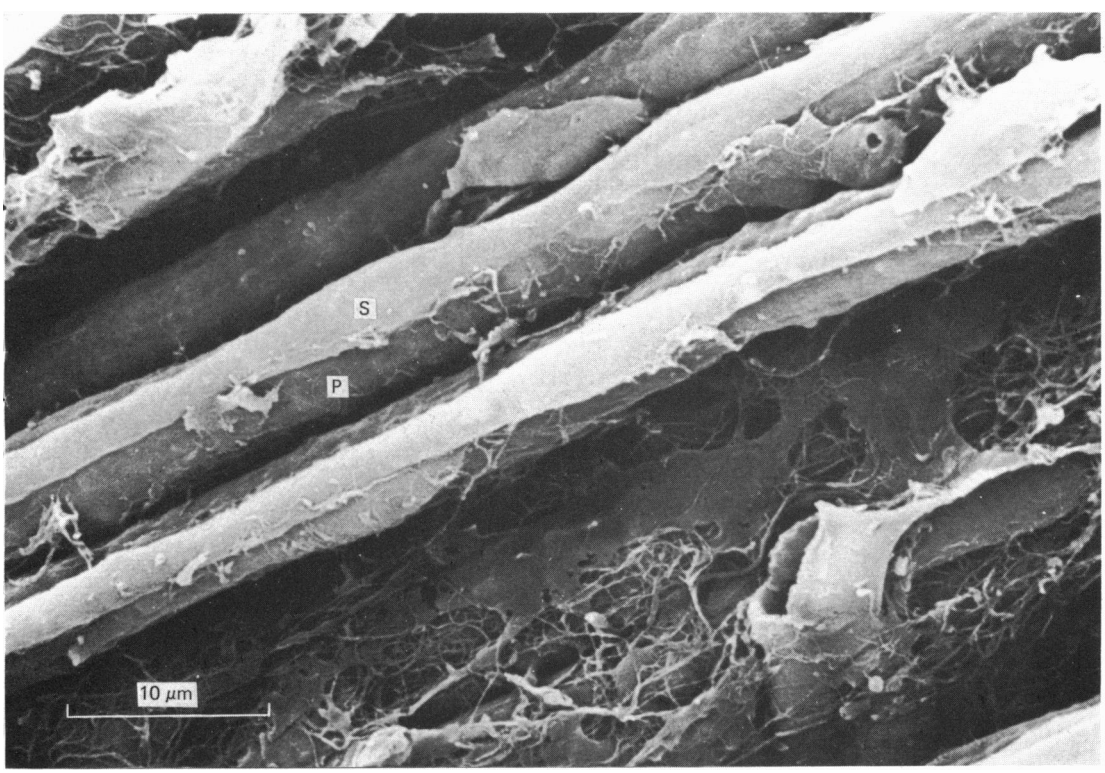

Fig. 8

attempted but did not produce such good results. The muscles were viewed on an ISI-60 scanning electron microscope.

At 12 days muscle tissue is difficult to distinguish whereas at 13 days long fibres are evident. Spindle shaped cells (myoblasts) can be seen in the crevices between adjacent fibres. At 16 and 17 days a population of secondary smaller fibres (Fig. 8, S) can be seen forming on the surfaces of the primary fibres (Fig. 8, P). At 18 days the fibres are more compact, with some fibres appearing more intimately associated with one another, possibly as the basal lamina enveloping adjacent primary and secondary fibres becomes more pronounced.

19. The postnatal development of rat cruciate ligament insertions. By C. F. KEARNS (introduced by A. J. PALFREY). *Department of Anatomy, Charing Cross Hospital Medical School, London*

The literature concerning the attachment zones of ligaments and tendons to bone is sparse considering their role in maintaining the integrity of the skeletal system. Biomechanical studies have shown that the region of transition between these tissues of different physical properties can withstand greater tensile forces than the bone immediately below it.

Hind limbs from rats 2, 5 and 10 days old, 2 months old and adult were fixed in Bouin's fluid. Where this procedure was not sufficient to demineralise the specimens, a patent decalcifying fluid (Bethlehem RDC) was used. Serial sections were stained with haematoxylin and eosin, periodic acid–Schiff, methyl blue/van Gieson and alcian blue (pH 2·5).

The postnatal development of the attachment zones can be conveniently divided into three phases. Initially the terminal ligamentous fibres are embedded in the epiphyseal cartilage matrix to form an intermediate zone of fibrocartilage. The second phase begins with the appearance during the second week of the secondary ossification centre. Cavities form throughout the epiphysis and the intervening areas of fibrocartilage become calcified. During the third phase, which begins after the second month, the calcified fibrocartilage is resorbed and replaced by lamellar bone. Thus in the adult rat the cruciate ligaments are attached to bone through a more superficial zone of fibrocartilage and a deeper zone of secondarily calcified fibrocartilage. The concentric nature of these layers reflects the developmental changes that originated in the epiphysis.

Basophilic lines mark abrupt boundaries between compact bone and calcified fibrocartilage and between calcified and unmineralized fibrocartilage. The nature of these lines is not clear. Periosteum does not intervene between the cruciate ligaments and bone but the superficial ligamentous fibres are continuous with the fibrous periosteum of the shaft of the long bones. These fibres are attached to neither the diaphysis nor the epiphyseal plate during growth.

20. The epithelium of accessory pancreatic ducts in the wild starling (*Sturnus vulgaris*). By S. VINNICOMBE (introduced by M. D. KENDALL). *Department of Anatomy, St Thomas's Hospital Medical School, London*

In the common starling, *Sturnus vulgaris*, a series of accessory pancreatic ducts runs into the distal limb of the duodenal loop; these have not been described in the literature. The aim of this study was to investigate the epithelium of these ducts, with particular reference to the presence or absence of any glands, and the nature of the underlying connective tissues.

Samples of the ducts from a series of five specimens (both males and females were included) were prepared for light and electron microscopy. Serial sections from samples fixed in Bouin's were stained with H & E, Heidenhain's azan, periodic acid–Schiff (with diastase control), alcian blue (critical electrolyte concentration method) and alcian blue+high iron diamine. Other sections, from samples fixed in 95% alcohol, were treated to ascertain the extent of alkaline phosphatase and acid phosphatase activity. Other samples were processed routinely for electron microscopy, but the extreme electron density of the epithelium, even under varied staining procedures, rendered characterization of the epithelium very difficult.

The epithelium consisted of a single layer of tall, columnar cells. The main cell type had a prominent nucleus with one nucleolus; its cytoplasm contained apical electron-dense granules; mitochondria; one or more para- or supranuclear dictyosomes; some SER, but virtually no RER. The epithelium showed a thin surface drape that was strongly reactive with PAS and alcian blue. This corresponded to short, apical microvilli embedded in a filamentous surface

coat that could be seen with the electron microscope. However, the apical granules appear non-reactive to any stains for mucosubstances.

A second, rarer, cell type, which appeared vesicular under the light microscope, had a large, convoluted nucleus with sparse cytoplasm. Its function is unclear.

21. The distribution of chondrocytes in human tracheal cartilage. By N. E. McCALLION, RUTH ST. C. GILMORE and A. J. PALFREY.* *Department of Physiology, The Queen's University of Belfast and *Department of Anatomy, Charing Cross Hospital Medical School, London*

In this study the number and distribution of chondrocytes in human tracheal cartilage have been investigated using a grid-counting method, planimetry and computer analysis. Pieces of trachea incorporating several rings above the carina were obtained from cadavers aged from 34 weeks gestation to 27 years. The tissue was fixed in neutral formol saline. Following routine paraffin processing, longitudinal sections were stained with haematoxylin and eosin or haemalum.

Sections were projected ($\times 250$) on to a screen marked out with grids of sides of 50 mm. The number of cells per grid in the middle area of the image was counted and the area of matrix per cell calculated. For planimetry, sections were projected on to a plain screen. Chondrocytes were selected at random and the area of matrix surrounding them mapped out. The area of these matrix 'domains', bounded by the cell's nearest neighbours, was measured.

Sections were analysed using a programmable flying spot microscope and picture preprocessor. Computer analysis of the image field enabled the number of cells and their nearest neighbour distances to be calculated. Total cellularity declined with increasing age, and within age groups was found to vary with position within the central area of the cartilage – moving from top to bottom of the rings minimum cellularity occurred at 50 % of total section length in neonates, 30 % in prepubertal children and at 20 % in adults.

Computer analysis of chondrocyte distribution identified cell clustering in all specimens. Younger cartilages showed little evidence of grouping based on first and second nearest neighbour distances, but third to fifth nearest neighbour distances indicated that the cells were not randomly dispersed. This grouping may have some function in determining the limiting thickness of cartilage which can be nourished by the surrounding vascular tissue.

Computer facilities were kindly made available by Dr D. Rosen, Department of Biophysics and Bioengineering, Chelsea College, London.

22. The ureteric epithelium of the wild starling (*Sturnus vulgaris*). By G. R. WILLIAMS (introduced, by M. D. KENDALL). *Department of Anatomy, St Thomas's Hospital Medical School, London*

Samples of ureter from five male and three female starlings (*Sturnus vulgaris*) were prepared for light and electron microscopy by conventional methods. Paraffin-embedded sections were stained with H & E, periodic acid–Schiff (PAS) and alcian blue for light microscopy. Thin sections were stained with lead citrate and uranyl acetate for electron microscopy.

At the light microscopic level individual cells were difficult to distinguish due to the presence of thick mucus which was highly PAS- and alcian blue-positive. Alcian blue histochemistry determined the presence of an acidic mucus containing both neutral and, predominantly, carboxylated acidic mucopolysaccharides. The epithelium was of tall pseudostratified columnar form throughout its length.

Under the electron microscope three cell populations were observed. A population of basal electron-lucent cuboidal cells each containing a central leptochromatic irregular nucleus; granular cytoplasm; few organelles, and cytoplasmic extensions extending into dilated intercellular spaces. The second cell type was composed of large, irregularly shaped, electron-dense, mucin-secreting cells extending from the lumen to basal cytoplasmic extensions. They contained crenated nuclei, highly proliferated and dilated rough endoplasmic reticulum, Golgi apparatus and many mitochondria, some of which were degenerate. They also contained many apical inclusions of mucus and these features were suggestive of holocrine secretion. A third population of intermediate cells with characters of both basal and mucin-secreting cells was also observed extending to the lumen.

These relationships between the cell types and their internal structures indicate the presence of a cell line from immature basal cells to the mature mucin-secreting cells with a variable population of intermediate cells.

23. Connections of the thalamic reticular nucleus in the adult rat: a study using horseradish peroxidase (HRP) techniques. By M. O'CONNELL, P. T. OHARA and A. R. LIEBERMAN. *Department of Anatomy, University College London* (Fig. 9)

The thalamic reticular nucleus (TRN) is a thin, curved sheet of cells surrounding the lateral and anterior aspects of the dorsal thalamus. It is penetrated by, and receives input from, the fibre bundles interconnecting the dorsal thalamus and the cerebral cortex, sends its output predominantly to the dorsal thalamus, and appears to play a role in monitoring and controlling the flow of information from the thalamus to the cortex.

To gain further insight into the organization of the TRN, its afferent and efferent connections were investigated by the HRP method, with special emphasis on the topographical organization of reticulothalamic projections. HRP (15 % in tris buffer) was injected iontophoretically from glass micropipettes (external diameter $\simeq$ 60 μm) positioned stereotaxically in various thalamic nuclei of anaesthetized adult albino rats. In several additional rats HRP was injected into the visual or somatosensory cortices. Animals were perfused with fixative 16–24 hours after injection. The brain was removed and sectioned at 40–60 μm in the frontal, horizontal or parasagittal planes. Series of alternate sections were processed for visualization of HRP using the DAB (diaminobenzidine) and the TMB (tetramethylbenzidine) techniques. The DAB material was used to define the injection sites and to determine the positions of cell bodies labelled by retrograde transport of HRP. The more sensitive TMB material was used both for this purpose and to determine areas of terminal labelling resulting from anterograde transport of HRP from the injection site. Fig. 9A shows an example of an injection site into the ventrobasal (VB) complex (frontal section, DAB) and Fig. 9B shows a patch of labelled cells in TRN following a similar injection (horizontal section, DAB).

Four major non-overlapping territories of cells projecting to ipsilateral dorsal thalamus were defined and are summarized in the simplified representation of TRN shown in Fig. 9C. The dorsocaudal region projects to the dorsal lateral geniculate nucleus (LGd), the dorsorostral region to the anteroventral (AV) and laterodorsal nuclei (LD), the ventrocaudal region to the medial geniculate nucleus (MG) and a large part of the ventral TRN anterior to the latter territory projects to the ventrobasal complex (VB). Cell populations projecting to other dorsal thalamic nuclei (e.g. to the lateroposterior and ventrolateral nuclei) lie between these projection territories. Anterograde labelling of axon terminals in the neuropil surrounding the retrogradely labelled cell bodies in TRN show reciprocal projections to TRN from the thalamic injection sites with a topography corresponding to that of the reticulothalamic projections. Anterograde labelling of terminals in TRN after HRP injections into cortex shows that the visual cortex projects to the part of TRN which receives input from LGd and that the somatosensory cortex projects to the part which receives input from VB.

24. Lymphocyte proliferative response to mitogen depends on macrophage content. By S. P. BARNARD and C. W. EVANS. *Department of Anatomy, University of St Andrews*

A requirement for macrophages has been demonstrated for various *in vitro* immune phenomena involving lymphocytes. These include the primary and secondary antibody responses and the mixed lymphocyte reaction, although the dependency for macrophages in the lymphocyte mitogenic response to lectins such as phytohaemagglutinin remains controversial. The problem appears to involve the identification and removal of residual macrophages in the lymphocyte population, so that the mitogenic response can be tested independently of macrophages.

A mixed population of lymphocytes and macrophages was isolated from mouse lymph nodes. Purification of the lymphocytes involved one or two nylon wool column adherence steps. A purified macrophage sample was obtained by allowing peritoneal exudate cells to adhere to a serum-coated petri dish. The adherent macrophages were subsequently removed by treatment with 5 mM EDTA at 4 °C. By centrifuging a sample of the cells and resuspending in 100 % serum, the staining of spread macrophages by the non-specific esterase histochemical technique was much improved.

One nylon wool column purification of the mixed peripheral lymph node cell population did not affect the PHA response, whereas two column purification steps abolished it. Loss of proliferation was not due to the isolation of an unresponsive subpopulation or to cell damage. The mitogenic response could be restored by reconstitution of the purified lymphocytes with as little

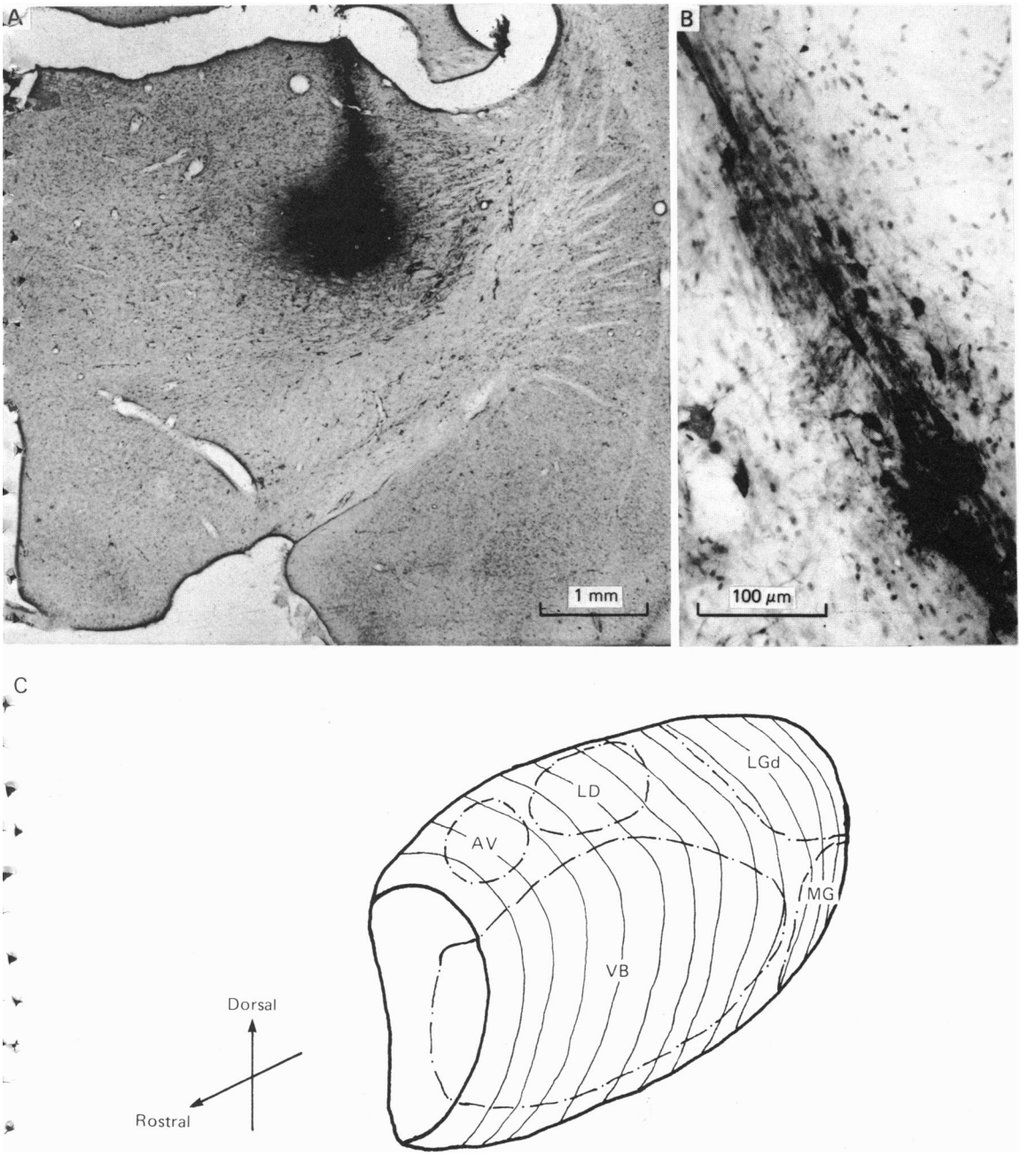

Fig. 9

as 3 % macrophages. Inhibition of proliferation was seen when the macrophage content exceeded 11 %. Both syngeneic and allogeneic macrophages restored the response at optimal concentrations.

The reconstitution of the mitogenic response by allogeneic macrophages is of importance in the light of recent work demonstrating a histocompatibility requirement in the immune response to antigen, and modulation of the mitogenic response by macrophages may underlie clinical manifestations of certain diseases involving the immune system.

25. The fetal vasculature of the human term placenta: a morphological study. By S. HABASHI (introduced by G. J. BURTON). *Department of Anatomy, University of Cambridge*

Although scanning electron microscopy of corrosion casts has provided much information on the microvasculature of many varied tissues (Hodde & Nowell, *S.E.M.* **11**, 1980), to the author's knowledge the technique has not previously been applied to the human placenta. In this study, casts of the fetal vasculature of 12 normal term placentae were produced by injecting chorionic vessels with an unsaturated polyester resin (Trylon Crystic Resin: Trylon Ltd, Wollaston, Northants). After corrosion of the placental tissues using concentrated hydrochloric acid, the resultant microvascular casts were dried, coated with gold/palladium and viewed in a Philips Stereoscan 600 microscope.

The most conspicuous feature of the casts was the presence of sinusoidally dilated capillaries, which often formed complex interlocking loops, producing a knot-like structure. The general disposition and closed-loop nature of these capillary knots suggested that they represented the vessels of terminal villi. This supposition was confirmed by the observation of such a knot actually within a terminal villus in an incompletely corroded specimen. Only the tissue overlying the maximally dilated regions of the capillary loops had been removed, indicating that at these points the vessels are normally overlain by a comparatively thin layer of trophoblast. Replicas of paravascular networks of capillaries surrounding larger villous vessels near the chorionic plate were also observed, as were casts of vasa vasorum.

By comparing the findings of this study with those obtained by conventional histological techniques, it was confirmed that the casts represented faithful replicas of the original luminal form of the fetal vessels. In conjunction with stereo-pair photography this technique enables rapid and unequivocal interpretation of the three dimensional configuration of the villous vasculature. It is hoped it may prove of assistance in the investigation of changes in the fetal vasculature which may occur in abnormal pregnancies.

26. Recent improvements in endoscopic techniques. By J. C. NICHOLLS (introduced by A. J. PALFREY). *Department of Surgery, Charing Cross Hospital, London and Hemel Hempstead Hospital, Buckinghamshire*

The 'modern' era of endoscopy began in 1958 with the introduction of the fibrescope by Hirschowitz. From early times the desire to visualize the interior of organs had been strong, but the physical limitations of the equipment made this impossible. The early part of this century saw the development of cystoscopy and gastroscopy.

Fibre-optic endoscopes rely upon the principle of total internal reflexion, which almost defies the principle of light travelling in straight lines. Recent improvements have been dependent upon refinements of the equipment, and ingenuity of the operators. There is now a range of endoscopes small enough to pass into the common bile duct, the ureters, the blood vessels, and large enough to allow therapeutic manoeuvres. Their flexibility and field of vision are almost unlimited, and they are long enough to reach from mouth to jejunum, and anus to caecum. Optical refinements have improved the light carrying ability, and the resulting view can be recorded on film and closed circuit television. The endoscopist now has the facility to pass biopsy forceps, cytology brushes, snares, needles, baskets and laser beams.

The techniques for performing upper and lower gastrointestinal endoscopy and for examining the bile ducts are now standard, and the risk to the patient is at a very low level.

The modern uses of endoscopy fall into two main categories. Diagnosis of diseases of oesophagus, stomach and duodenum, rectum and colon can be made by direct observation and proof obtained by biopsy. In combination with radiological techniques the biliary tree and pancreas can be examined for disease. Therapeutic applications of endoscopy are constantly widening. Dilatation of oesophageal strictures, control of gastrointestinal haemorrhage, removal of bile duct stones and excision of colonic polyps are an example of such applications. The place of endoscopy in screening for disease is not yet established.

27. photogrammetric techniques. By L. F. H. BEARD (introduced by A. J. PALFREY). *Medical Photography and Illustration Service, Addenbrooke's Hospital, Cambridge*

A stereopair of photographs contains comprehensive and accurate information on the size and shape of the subject recorded. However, delays occur in gaining access to this information because of the procedures involved in reorientation of the stereopairs in the plotting equipment. These delays, together with the scarcity of the skill required for taking measurements from a spatial model, has hindered the replacement of traditional methods of measurement by stereophotogrammetry. The design of a stereometric camera/plotter for clinical photography based on non-metric cameras and lenses has minimised problems of reorientation. Methods of simplifying analysis have also been devised. The results of these developments, and their applications, were described and demonstrated.

28. The contribution of nuclear medicine. By E. S. WILLIAMS (introduced by A. J. PALFREY). *Institute of Nuclear Medicine, The Middlesex Hospital Medical School, London*

Radiation-emitting atoms can be incorporated into, or attached to, molecules, colloid particles, cells, and so on, thus enabling the distribution of these materials in the body to be delineated by suitable radiation detection instruments. It is important to note that the medically useful information is provided by how the body handles such a radioactively labelled material. The choice of label, the radioactive isotope, is a complicated one, but is a largely technical problem.

A common form of the presentation of results is in the form of an 'image' of the distribution in the body of the radioactive material which has been administered. However, it must be emphasised that this is a functional image representing an aspect of the physiological state of the organ or part of the body being studied. For example, if a radioactive colloid is introduced by intravenous injection the colloidal particles are rapidly cleared by the cells of the reticulo-endothelial system and, because of the concentration of these cells in the liver, an image of the liver can be obtained. If this cellular system has been damaged (e.g. after recent radiotherapy to the liver) then no image will be obtained. This is a dramatic illustration of imaging the functional nature of a nuclear medicine image.

This property sets nuclear medicine imaging apart from other imaging modalities, such as the use of ultrasound, or X-rays which, while they demonstrate anatomical structures, give no information on the functional state of those structures. An example is provided by disease of bone. If the bone is only slightly decalcified by the disease, then it could well present a normal X-ray image. However, if its metabolic state is affected this might easily be detected early in the progress of the disease by the use of an appropriate bone-seeking agent and the production of a nuclear medicine functional image.

29. Xeroradiography. By A. J. STACEY (introduced by A. J. PALFREY). *Department of Physics Applied to Medicine, Charing Cross Hospital, London*

Xeroradiography is a relatively new X-ray technique in which a specially prepared Xerox plate is used instead of X-ray film. It is becoming accepted in mammography, and is establishing its place in the examination of other anatomical sites.

The radiological image on the Xerox plate is characterized by the so called 'edge effect', which results in pictures bearing remarkable resemblances to line drawings. It also exhibits a wide exposure latitude and one X-ray exposure can be used to display tissues of widely differing radiation properties.

The method of image formation was outlined and the limitations imposed by the radiation dose to the patient were considered. Examples were shown to illustrate the significant properties of the Xeroradiographs and also to indicate the range of clinical application.

Other electrostatic systems are being developed and the principal features were discussed. Future improvements which may be expected of these methods were also reviewed.

30. Recent trends in interventional radiology. By J. MCIVOR (introduced by A. J. PALFREY). *Department of Diagnostic Radiology, Charing Cross Hospital, London*

It is now possible for the radiologist to pass needles and catheters into most large organs and into the blood vessels which supply them. These procedures provide anatomical demonstrations which were unobtainable in the living until recently. A knowledge of normal anatomy and of the common variations is of course a pre-requisite for technical success and for diagnostic accuracy.

In addition to diagnostic procedures, therapeutic measures, such as drainage of obstructed biliary and renal tracts, occlusion of the arteries supplying tumours and arteriovenous malformations and the dilatation of narrowed arteries, are now regularly undertaken.

This paper showed examples of these newer techniques and discussed their role in the management of patients.

31. Isolation of structures at the basement membrane zone of normal human skin. By J. NANCHAHAL, D. J. RICHES* and T. W. GLENISTER. *Department of Anatomy, Charing Cross Hospital Medical School, London, and *Department of Anatomy, Chinese University of Hong Kong*

The isolation of human cutaneous basement membrane (BM) has previously been attempted by Heaphy & Winkelmann (*J. Invest. Derm.* **68**, 1977), but their final preparation showed considerable collagen contamination. All biochemical analyses of cutaneous BM have been performed on partial enzyme-digests of whole skin and so this study was undertaken to obtain an ultrastructurally 'pure' sample of cutaneous BM for analysis.

Areas of normal human skin, about 8 × 30 cm, were obtained from patients undergoing plastic surgery and were soaked in 2 M-NaSCN for 5 hours at 4 °C. This permitted the epidermis to be peeled away, leaving the BM intact on the dermal surface. The latter was intermittently ultrasonicated in the presence of 0·3 % Triton X-100 in phosphate-buffered saline (PBS) for 45 min in an ice-bath. A fraction enriched in BM was obtained from the PBS suspension using differential centrifugation and discontinuous CsCl density gradients. All stages were monitored by electron microscopy.

The NaSCN appeared to disrupt selectively the structures at the lamina lucida (hemidesmosomes) whilst the desmosomes remained intact; this may reflect an intrinsic chemical difference between these two structures. The dermal cells were disrupted and the cytoplasm of the epidermal cells was very electron-dense whilst their nuclei became electron-lucent. In the presence of enzyme inhibitors, flocculent material (at least in part of nuclear origin) was attached to the BM and in centrifugates two types of BM could be identified:

(i) 'light BM' – similar to that in normal tissues, but which stained less intensely.
(ii) 'dark BM' with flocculent material attached to it.

In the absence of Triton X-100, very vigorous ultrasonication was required to release the BM, which showed marked variation in thickness. During the purification steps the BM appeared to break up, but the bond between the BM and anchoring fibrils was found to be very resilient. However, in the absence of enzyme inhibitors profiles of BM without anchoring fibrils were common and occasionally the BM was seen to split into three layers.

Preliminary analyses have shown the final fraction to consist of *c.* 75 % basement membrane and anchoring fibrils by mass.

32. Studies on hemolymph nodes: the intrinsic vasculature of the renal hemolymph node of rats. By AVRIL M. PEARCE, O. REID and R. J. SCOTHORNE. *Department of Anatomy, University of Glasgow*

Unlike those of 'typical' nodes, the lymph sinuses of hemolymph nodes contain abundant erythrocytes. Nopajaroonsri, Luk & Simon (*J. Ultrastruct. Res.* 1974) claimed that the hemolymph node was more vascular than typical nodes and that erythrocytes entered its sinuses by diapedesis through intrinsic capillaries and venules. We have compared the intrinsic vasculature of the renal hemolymph node with that of the facial node of the rat, using thick cleared sections after intravascular perfusion with alcian blue, and semithin plastic embedded sections.

The vascular pattern was essentially similar in the two types of node. Arterioles extended radially from the hilum, to supply principally a deep plexus at the corticomedullary junction

and a richer subcapsular plexus. These plexuses drained into postcapillary venules and thence, via high endothelial venules (HEV), to segmental and collecting veins.

Differences between vascular patterns in the two nodes may be related to the fact that the facial node is the more active immunologically, for:

(i) Arteriovenous anatomoses were more numerous in the facial node.

(ii) HEVs were consistently more numerous and larger in the facial node.

(iii) The subcapsular and corticomedullary plexuses were richer in the facial nodes, although their patterns were distorted by more numerous and (avascular) germinal centres and by larger (and relatively avascular) paracortical nodules of the thymus-dependent zone.

Counts of cells migrating through the walls of HEV show comparable, very large, numbers of lymphocytes and very small numbers of erythrocytes in the two nodes. The results do not support the view that significant numbers of erythrocytes enter the lymph sinuses by an intrinsic route.

33. Origin of matrix vesicles of developing dentine investigated by freeze-fracture. By E. KATCHBURIAN and N. J. SEVERS*. *Department of Anatomy and Histology, The London Hospital Medical College, London, and *Department of Cardiac Medicine, Cardiothoracic Institute, London* (Fig. 10)

Matrix vesicles are cell-derived membrane-bound bodies which have been demonstrated in ultrathin sections by electron microscopy in the matrix of dentine during early dentinogenesis (Fig. 10, arrows). The vesicles lie free in the matrix and are limited by a membrane which exhibits a typical trilaminar structure. When mineralization of dentine begins, the first mineral deposits appear as crystal-like inclusions inside the matrix vesicles, an observation which led to the proposition that matrix vesicles act, in some way, as promoters of calcium phosphate precipitation (Katchburian, *J. Anat.* **116**, 1973). Although of cellular origin it is not known whether matrix vesicles form by budding off from the surface of odontoblasts or by extrusion of some intracytoplasmic precursor. To investigate the origin of matrix vesicles we have examined developing dentine in specimens prepared by freeze-fracture.

Molar tooth germs from 3 days old rats were fixed in cacodylate-buffered 4 % glutaraldehyde–4 % formaldehyde and were then treated with cacodylate-buffered 25 % glycerol. The specimens were frozen in propane and fractured in a Balzers BAF 400T apparatus, and the replicas were examined in a Jeol JEM 100B electron microscope.

Early developing dentine shows typical criss-crossing collagen fibres which appear as plastically deformed stubs in transverse fractures and as striated structures in longitudinal fractures (Fig. 10). Portions of odontoblast processes (Fig. 10, P) and matrix vesicles (Fig. 10, M) are present in the intercollagenous regions. The membranes of odontoblast processes reveal a density and distribution of intramembrane particles on the P- and E-faces which is indistinguishable from that observed on the membrane fracture face of matrix vesicles. This is consistent with the idea that matrix vesicles probably arise by budding off from the surface of odontoblast processes. We are currently investigating the possible changes which may take place in the membrane of matrix vesicles during calcification.

34. Radiation-induced giant epithelial cells in small intestinal mucosa. By K. E. CARR, R. HAMLETT*† and C. WATT. *Department of Anatomy, Glasgow University and *Radiobiology Research Group, Belvidere Hospital, Glasgow*

Structures which were interpreted as 'giant enterocytes' were identified in a scanning electron microscope study of the effects of irradiation on mouse small intestinal mucosa (Carr *et al. J. Microsc.* **123**, 1981). Their histology and ultrastructure have now been studied in more detail. A sample of 22 adult C_3H/He mice, made up of both sexes, were irradiated with either 10 Gy X-rays or 5 Gy neutrons, and areas of mucosa were examined 5 days later by light microscopy, transmission electron microscopy (TEM) and scanning electron microscopy (SEM). In 8 of the 22 mice, SEM revealed flat or pedunculated swellings, 25–60 μm in width, situated at various levels of the surface of the villus. The surface was smooth, and showed neither cell boundaries

† Present address: University of Oxford Research Institute, Churchill Hospital, Oxford.

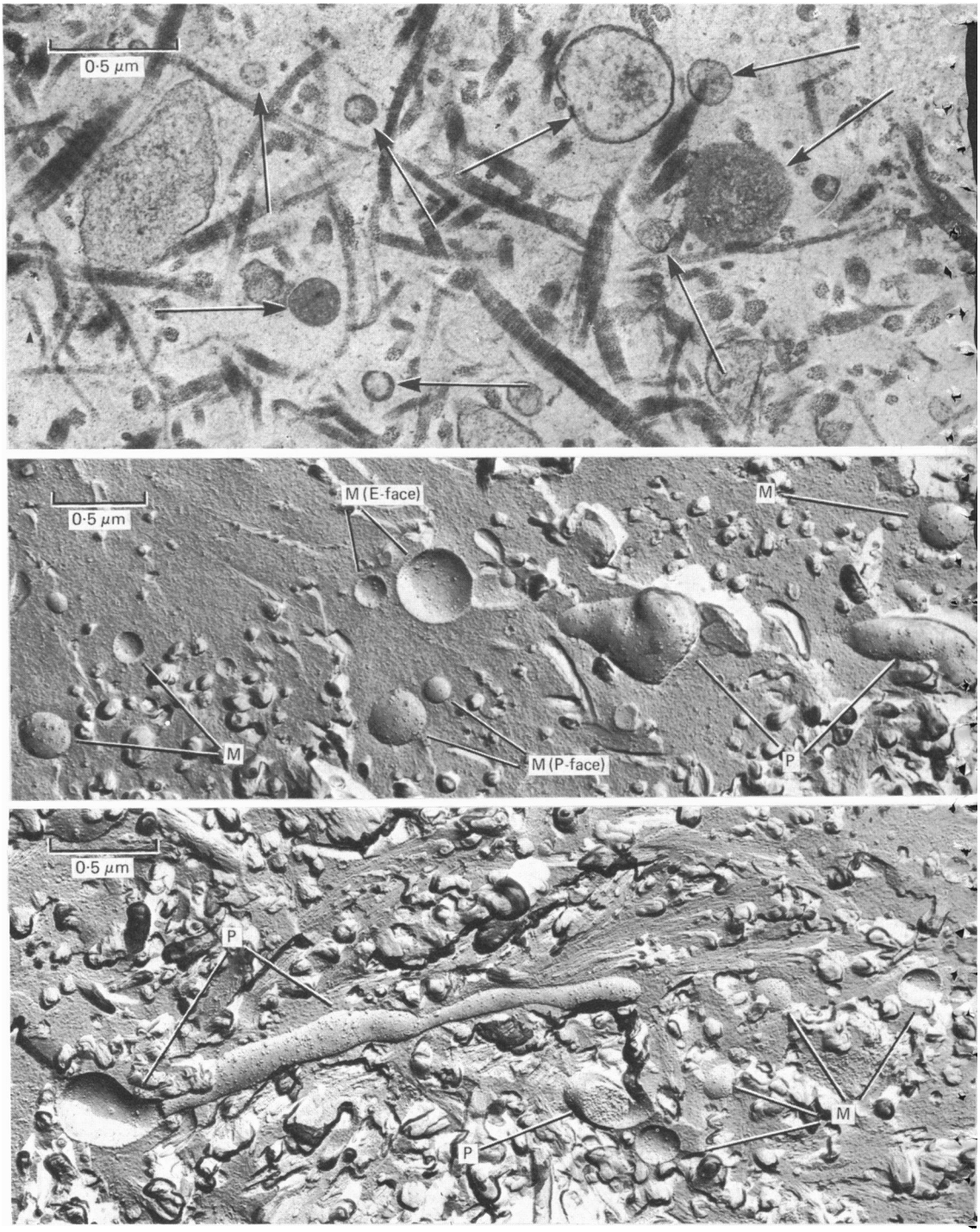

Fig. 10

nor evidence of discharging goblet cells. in semithin sections, the swellings consisted of a multinucleate mass of cytoplasm lacking cell boundaries, containing large vacuoles and PAS-positive granules which we have interpreted as mucus. Contact with stroma and adjacent epithelial cells appeared complete.

Transmission electron microscopy showed apical microvilli to be sparser than on normal enterocytes. The cell membrane showed basal herniations, and exaggered lateral interdigitations. Intracytoplasmic vacuoles lined by trilaminar unit membranes were seen, as were occasional intracytoplasmic desmosomes. Lipid inclusions were conspicuous, as they were in the radiation damaged enterocytes.

The swellings show some features of both absorptive cell and goblet cell differentiation. The significance of their structural peculiarities is discussed in relation to irregularities of mitotic division and differentiation of the stem cell population.

35. The muscularis mucosae of the human urinary bladder. By J. S. DIXON and J. A. GOSLING. *Department of Anatomy, University of Manchester*

Standard histological textbooks (e.g. Ham's *Histology*) describe the mucosa of the urinary bladder as consisting of a layer of transitional epithelium and a supporting layer of loose connective tissue (the lamina propria) and make no mention of a muscularis mucosae. Indeed some texts state categorically that a muscularis mucosae is absent from the human urinary bladder (e.g. *Gray's Anatomy*). During studies on the human lower urinary tract we have recently had the opportunity to examine a number of normal bladder biopsy samples removed from a variety of sites, including the fundus, the anterior and lateral walls and the trigone. In all cases the biopsy samples were examined using both light and electron microscopy.

Irrespective of site, the bladder wall was observed to possess an incomplete layer of smooth muscle separated by loose connective tissue from the basal aspect of the urothelium and also the inner aspect of the detrusor muscle, thus corresponding to a rudimentary muscularis mucosae. The constituent cells of this muscle layer could be clearly distinguished both histochemically and ultrastructurally from detrusor smooth muscle cells. The cells are rich in non-specific cholinesterase and react positively when stained with the periodic acid–Schiff technique. In the electron microscope the smooth muscle cells are extremely irregular in outline and contain large areas of sarcoplasm packed with electron-dense glycogen granules. Numerous acetylcholinesterase-containing nerves course between the smooth muscle cells of this muscularis mucosae; in the electron microscope, varicose axon terminals containing small (50 nm diameter) agranular and occasional large (100 nm diameter) granulated vesicles are observed in close proximity to the smooth muscle cells.

36. Histological observations on the effects of localised hyperthermia on normal pig striated muscle. By D. J. RICHES, B. M. SOUTHCOTT*, P. B. DUNSCOMBE† and K. GAMMAPILA†. *Department of Anatomy, The Chinese University of Hong Kong and Departments of *Radiotherapy and Surgery, and † Medical Physics, Charing Cross Hospital, London*

The recent clinical application of hyperthermia produced by microwave radiation in the treatment of tumours has prompted an investigation to establish at what temperature damage occurs in normal tissue. Preliminary results have shown that maintaining deep temperatures in excess of 45 °C for 30 minutes produced observable effects. As there is a temperature gradient across the area covered by the applicator, approx. 10 cm × 6 cm, with a central peak, a method for measuring the deep (i.e. subcutaneous fat/muscle interface) temperature at 1 cm intervals using thermocouples was devised, thus enabling a study of the effects of varying temperature.

Hyperthermia was induced in the gluteal region of anaesthetized pigs, using microwave radiation at 434 MHz for 30 minutes. The skin was cooled by air blown between the applicator face and the skin. Both skin and deep temperatures were continuously monitored. Punch biopsies of skin and underlying muscle were taken across the treated area 1 and 6 weeks after treatment. The tissues were processed for both light and electron microscopy.

At 1 week after treatment, muscle fibres that had been heated to 48 °C were obviously damaged, with loss of nuclei and coagulation of myofibrils. Similar effects, but to a lesser degree, were seen at 47 and 45 °C. At lower temperatures the muscle fibres appeared relatively normal,

with only slight separation of the myofibril bundles. By 6 weeks after treatment, the area of muscle heated to 48 °C showed signs of recovery. The fibres were swollen, but nuclei were present, some being 'trapped' within the fibres. In the other areas, the fibres were also recovering, but there was marked lymphocytic infiltration in all regions.

Although the effects of hyperthermia described are non-specific, these preliminary results demonstrate that muscle fibres can recover even after being heated to 48 °C. Further studies are in progress at the ultrastructural level to establish the detailed effects both on the myofibrils and the microvasculature.

37. The physics of tomographic techniques. By J. S. ORR (introduced by A. J. PALFREY). *Department of Medical Physics, Royal Postgraduate Medical School and Hammersmith Hospital, Du Cane Road, London*

Tomography is the process of representing an object by a series of pictures in the form of sections or slices. The process has three components. First, measurements of properties of the object, either as a point, or as a small volume, must be made. Second, the point, or volume, must be localised in the slice. Third, interference from material elsewhere in the object, or slice, must be eliminated or reduced. Under certain conditions tomography is preferable to techniques which produce total projection images.

A wide range of properties can be measured: radioisotope concentration, X-ray or particle attenuation and magnetic resonance properties. Localisation commonly depends simply on the linear propagation of rays. Reduction of interference is often produced by blurring detail from elsewhere in the object, and physicists have devoted considerable efforts to refining the last procedure. The modern techniques of magnetic resonance imaging illustrate most of the essential features of tomography.

38. Nuclear magnetic resonance imaging. By G. M. BYDDER and I. R. YOUNG (introduced by A. J. PALFREY). *Royal Postgraduate Medical School, Hammersmith Hospital, London*

A description of a nuclear magnetic resonance (NMR) imaging system was presented together with some results from its clinical evaluation. The detection of proton magnetisation within a static magnetic field is outlined, and the rotating frame is used to describe the motion of the magnetisation. Radiofrequency pulses are used to rotate the magnetisation and slice selection is achieved using a 90° pulse and a magnetic field gradient. Three scanning modes are described: repeated free-induction decay (FID), inversion-recovery and spin-echo. These sequences produce images whose pixel values have different dependencies on proton density, T_1 and T_2.

Inversion-recovery images show striking differentiation between grey and white matter in the brain. The absence of bone artefact is a significant advantage over X-ray computed tomography in the posterior fossa where rapid repeated FID sequences can also be used to demonstrate flow effects.

Blood within the left ventricular cavities is differentiated from myocardium, and the paramagnetic effects due to dissolved arterial oxygen can be demonstrated.

The considerable soft tissue contrast available with NMR is of value in demonstrating disease within the liver where T_1 appears to be a sensitive, but relatively non-specific, diagnostic parameter. The cortex and medulla of the kidney can also be distinguished. High resolution scans are of value in demonstrating the adrenal gland and spinal cord.

Although the spatial resolution of NMR scanners is not as good as that of third and fourth generation computerised tomography scanners, the high level of soft tissue contrast, and absence of bone artefact, enable a variety of structures to be visualised in a way not possible with other imaging techniques.

39. Computerised tomography (CT). By D. E. KATZ (introduced by A. J. PALFREY). *Department of Radiology, Northwick Park Hospital and Clinical Research Centre, Harrow, Middlesex*

Computerised tomography is a technique which utilizes a conventional X-ray beam and, with the aid of highly sensitive detectors and computers, produces a cross sectional image at any desired level of the body.

The technique requires a tightly collimated X-ray beam to rotate around the patient, and, for each section detectors obtain over 300000 absorption measurements at a variety of angles.

The computer converts this raw data into a set of profiles and the main part of the computer processing then converts these profiles into information which can be displayed as a picture.

Computerised tomography overcomes many of the main limitations which have been imposed on conventional radiology for almost a century. By summating the cross sectional images it is possible to present three dimensional information about the internal structure of the body. The sensitivity of the recording apparatus makes it easy to distinguish between the soft tissues of the body, and gives a clear anatomical display of organs such as liver, pancreas and spleen.

Computerised tomography also allows quantitative differentiation by measuring X-ray absorptions of the different tissues. In addition it allows detailed examination of all tissues so that in a single section tissues such as lung parenchyma, mediastinal soft tissues and bone can all be scrutinised.

The anatomical limits are imposed by the spatial resolution and density resolution and these two are limited by the radiation dose.

The greatest impact of computerised tomography has been in neuroradiology, but the ability to display the whole body has created a new dimension in non-invasive investigative imaging of the body to be used in conjunction with other scanning techniques.

40. Microfocal radiography: a new X-ray technique for high resolution quantitative macroradiography of human extremities. By J. C. BUCKLAND-WRIGHT. *Department of Anatomy, Guy's Hospital Medical School, London*

Fine X-ray sources (5–10 μm diameter) have been used with some success in the detailed radiographic examination of the structural organisation of normal and diseased tissues. The relatively low energy levels necessary for ultra-small X-ray sources results in long X-ray exposure times which have hitherto limited its use to small live animals and *post mortem* animal and human material. However, recent advances in the design of microfocal X-ray equipment has resulted in a new high energy unit suitable for the routine radiographic examination of patients.

This new X-ray unit operates at 60 kV, 1 mA with an estimated X-ray source size of 6–8 μm diameter; this is, to date, the smallest known source at these energy levels. The operation of this unit in conjunction with the new rare earth film/screen combinations (Trimax) permits macroradiographic examination of the extremities of patients with an object resolution in the film of 25–35 μm at magnifications up to $\times 10$. Exposure times are between 0·7 and 1 second. The X-ray dose is within clinically acceptable limits of 34–70 mR/exposure. As penumbral blurring is minimal and all planes of the object are in focus, stereopair radiographs provide three dimensional assessment of structures with greater radiographic detail than obtained hitherto.

The microfocal X-ray unit is currently used clinically for diagnosis and investigative work. In the former, it is used in the precise identification of osseous changes associated with metabolic bone disorders and in the different types of arthritis. The latter consists of long term quantitative analysis of groups of patients with (*a*) early rheumatoid arthritis (to study the onset and enlargement of erosions), (*b*) rheumatoid arthritis with well developed erosive arthropathies, to assess the effectiveness of treatment, (*c*) osteoarthritis and (*d*) the levels of osteoporosis and the effect of phosphate binders in children with renal osteodystrophy. Because of the large magnification and high resolution in the macroradiographs, quantitative assessment of the changes observed are readily obtained by direct measurement using an image analyser.

41. The sex of *Alligator mississippiensis* is determined by the temperature of egg incubation. By M. W. J. FERGUSON. *Department of Anatomy, The Queen's University of Belfast* (Fig. 11)

Heteromorphic sex chromosomes are absent in all crocodilians. The effect of egg incubation temperature on sexual differentiation was investigated in laboratory and field experiments. 500 alligator eggs were collected from wild nests in the swamps of Louisiana and incubated at either 26, 28, 30, 32, 34 or 36 °C. After 60 days (alligators normally hatch at 65 days) eggs were fixed in 10% formalin. The alligators were examined under a dissecting microscope for the presence or absence of an oviduct or vas deferens and for the external shape and surface features of the gonad. The entire reproductive systems of 100 animals were serially sectioned at 8 μm in the horizontal, transverse and sagittal planes. In all cases where an oviduct was present the gonad was an ovary, when absent it was a testis. Sex is therefore fully determined in the embryonic period, and can be assayed by the presence or absence of an oviduct. Eggs incubated at, or below, 26 °C and

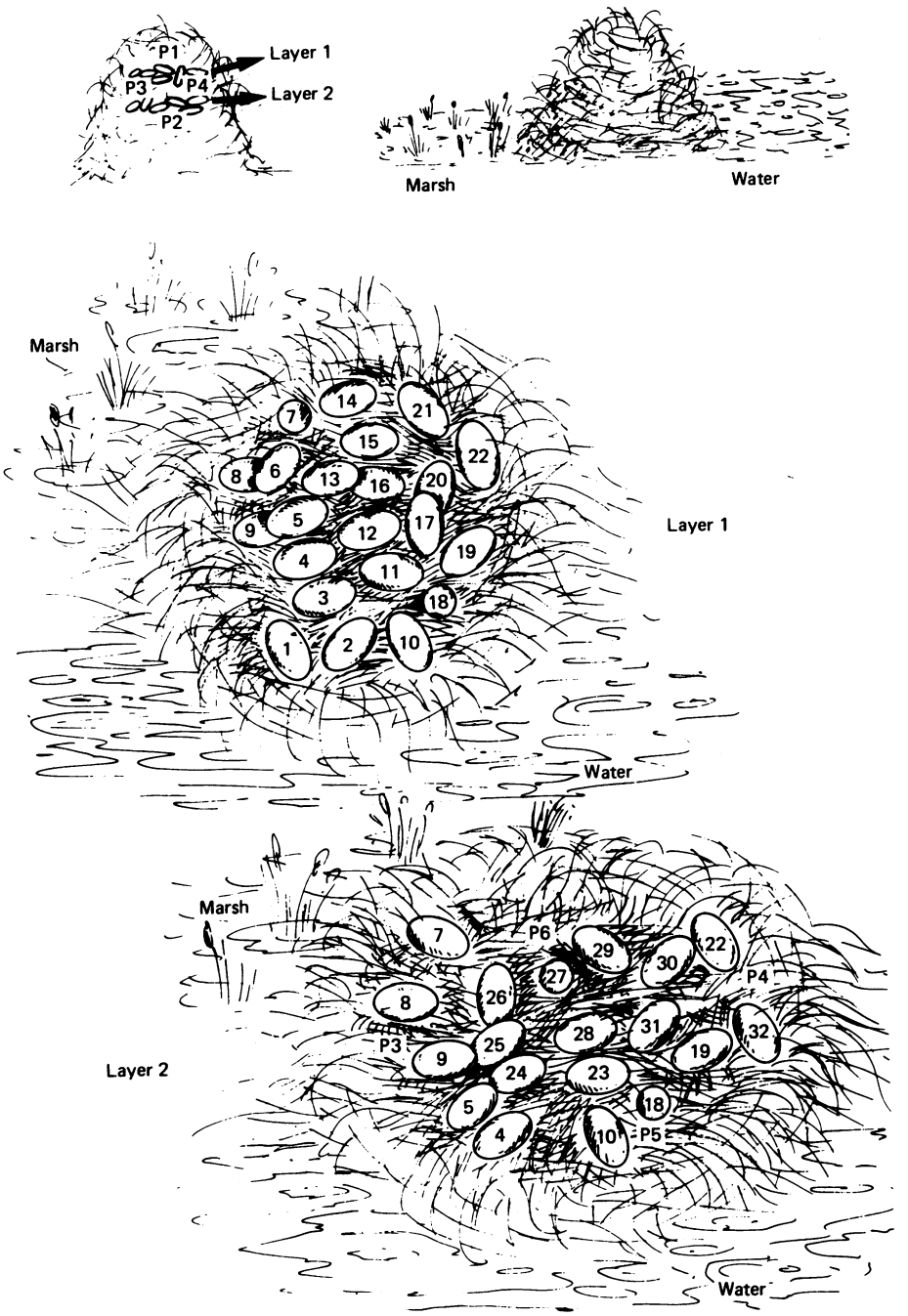

Fig. 11. P1, 34 °C; P2, 31 °C; P3, 32 °C; P4, 30 °C; P5, 31 °C; P6, 30 °C.

at, or above, 36 °C died. 100 % of eggs incubated between 28 and 30 °C were females and 100 % of eggs incubated at 34 °C were males. Eggs incubated at 32 °C yielded 86 % females and 14 % males. The average mortality was 6 % and there was no significant difference between the four temperature groups (28, 30, 32 and 34 °C).

Nest temperatures were continuously chart-recorded for eight wild alligator nests (four constructed in the marsh and four on levees) with probes (P1–P6) at the top (P1), sides (P3–P6), and bottom (P2) of the egg cavity (Fig. 11). A map of egg position within the nest was drawn when the eggs were fixed at 60 days (Fig. 11). All levee nests recorded average temperatures of 34 °C or above, at all locations in the nest and 100 % of the eggs developed into male alligators. All wet marsh nests recorded temperatures of 30 °C or below and 100 % of the eggs yielded females. Intermediate dry marsh nests recorded varying temperatures (Fig. 11). Male alligators developed from the hottest location in the nests – top central layer (Fig. 11, eggs 12, 13 and 16) and female alligators from the cooler locations – periphery and bottom (Fig. 11, eggs 1–11, 14, 15, 17–32). Laboratory experiments in which alligator eggs were incubated at a female-producing temperature for the first x stages of development and then shifted to a male temperature for the remainder of development (or *vice versa*) showed that the temperature-sensitive period for sex determination is within the first 3 weeks of incubation. A 4 years study of the sex of all hatchling alligators (n = 6000) within an extensive area of normal habitat revealed that the natural sex ratio at hatching is 6 females : 1 male. Given this natural skewed sex ratio, theoretical calculations show that genotypic influences probably have little effect on sex determination. Animals raised for 4 years after hatching showed no sex reversal. In both laboratory and field experiments, the weight of males at hatching was significantly less than that of females. Given the reproductive biology and natural history of alligators it can be shown that this constitutes a selective biological advantage for temperature-dependent sex determination over possible genotypic mechanisms. Temperature-dependent sex determination in alligators has many implications for embryological, teratological and molecular investigations as well as for conservation planning and farming. It may also provide a clue to the mechanism of extinction of other archosaurs, e.g. dinosaurs.

This work was supported by M.R.C. Grant No. G979/386/C, E.H.S.S.B. grant no. EP109/74/75 and a Wellcome Trust Research Travel Grant.

42. Venous drainage of the ovine corpus cavernosum penis. By R. R. ASHDOWN, S. W. BARNETT and G. ARDALANI. *Department of Anatomy, Royal Veterinary College, University of London* (Fig. 12)

Studies on various Artiodactyla suggest that drainage of the corpus cavernosum penis (ccp) by the v. dorsalis penis occurs only in young or impotent animals. In the goat, however, anastomoses between an intracorporeal 'v. trunci penis' and the corpus spongiosum glandis (csg), have been described draining the ccp (Starflinger, *Anat. Histol. Embryol.* 1, 1972). These anastomoses would be of functional and clinical importance, and we therefore examined the angioarchitecture of the excised penile bodies of 28 rams all aged 5 months or more, so that separation between penile integument and prepuce was completed.

Erection was simulated by the injection of Colorpaque or Micropaque at 40 °C into the dorsal canal of the ccp at known reservoir pressures (23 specimens). Straightening of the penis was completed at 210×10^3 Pa. At 350×10^3 Pa, mean total length had increased by 37·3 % and mean diameters by 3·0 %.

Two small specimens showed traces of injected material in the v. dorsalis penis at, or just distal to, the sigmoid flexure; these were the smallest specimens examined (total lengths before injection – 28·8 and 30·1 cm). In all other specimens, radiography and clearing in methyl salicylate failed to demonstrate venous drainage from the ccp. Anastomoses with the corpus spongiosum penis (csp) or csg were not demonstrated in any specimen (Fig. 12).

Incremental injections into the ccp and csp (five specimens) showed that the csp drained via the tuberculum spongiosum and csg into the v. dorsalis penis, but showed no connections with the ccp. The 'v. trunci penis' was a secondary dorsal canal of the ccp, having no anastomoses with vessels outside the tunica albuginea. Our experiments suggest that absence of venous drainage within the penile body facilitates the rapid generation of high pressures in the ccp by minimal flow volumes. When the distal bend of the sigmoid flexure began to straighten, only a further 7–12 ml of blood were needed to complete this straightening and then produce stiffening with maximum elongation of the organ.

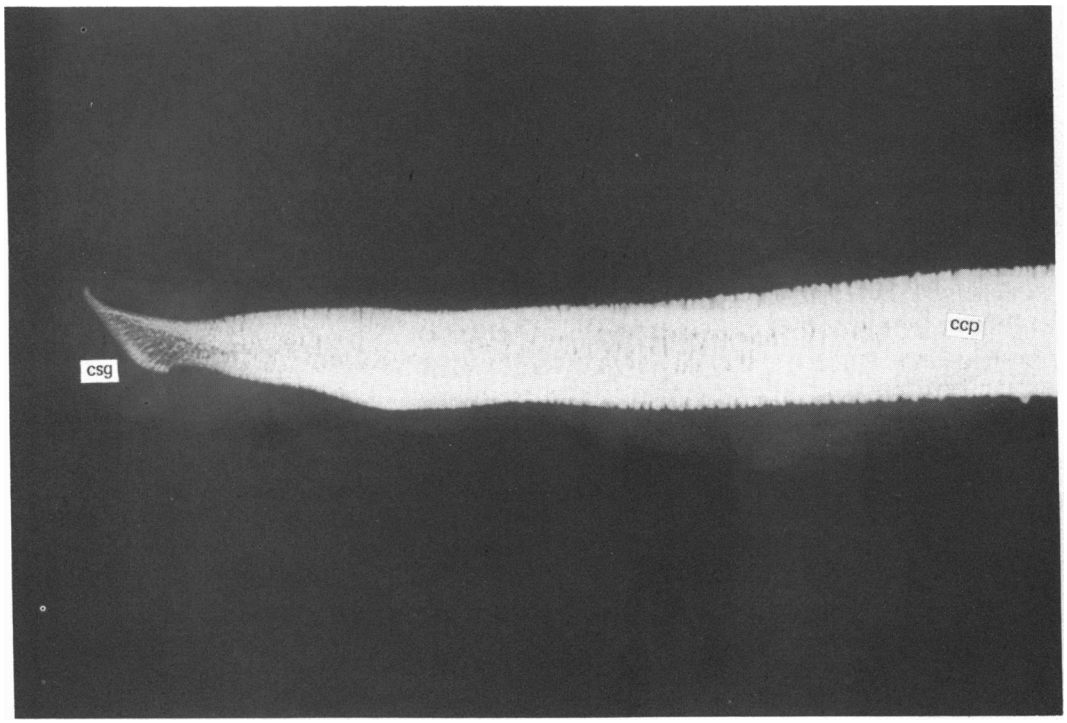

Fig. 12

43. A comparison of the anatomy and biomechanics of the ankle in normal infants, and those with club foot. By S. W. HOSKING and W. SCOTT* (introduced by A. J. PALFREY). *Department of Anatomy, Charing Cross Hospital Medical School and *Department of Orthopaedics, Charing Cross Hospital, London*

Several studies of the anatomy and biomechanics of the ankle region have been carried out on living and cadaveric adults. No biomechanical studies have been reported using infants. Our study was undertaken using specimens from cadaveric infants to determine (1) normal anatomy and biomechanics, (2) anatomy and biomechanics of club foot and (3) to make a comparison between normal and clubbed feet.

Three normal feet and three feet exhibiting talipes equino varus from stillborn infants were dissected. The tibiae were immobilized in a bench clamp while the range of dorsiflexion was studied before, and after, immobilization of either the medial, or lateral, or both, groups of tendons in the ankle region. Movements at the subtalar and talocrural joints were studied as well as factors controlling movements at the subtalar joint.

The normal specimens of infants were anatomically similar to the adult but important differences were found in the clubbed feet which may be relevant to subsequent biomechanical studies. Biomechanical studies showed that in normal specimens minimal movement occurred at the subtalar joint during dorsiflexion. When the anatomical abnormalities of club foot were simulated in the normal specimen, the characteristic inversion and plantarflexion seen in club foot was reproduced. Partial correction of the abnormalities (as practised in clinical surgery) resulted in a partial increase in dorsiflexion. Correction of those abnormalities that prevented subtalar movement resulted in the greatest increase of foot movement.

It is suggested that the role of the subtalar joint in normal feet is minimal during dorsiflexion. In partially corrected club foot, with its associated abnormalities, subtalar movement is essential to increase the range of foot movement, particularly eversion and dorsiflexion. Anatomical factors controlling movement at the subtalar joint in club foot have been demonstrated and are of importance in attempting to increase the limited range of movement exhibited by this deformity.

44. The use of ultrasound in medical diagnosis. By H. B. MEIRE (introduced by A. J. PALFREY). *Division of Radiology, Northwich Park Hospital and Clinical Research Centre, Harrow, Middlesex*

Diagnostic ultrasound techniques rely on the extraction of information from the echoes produced by internal structures during insonation with high frequency sound. Although early clinical results were obtained over thirty years ago the technique has only found wide clinical application during the past decade, with particularly rapid growth during the past five years.

Modern ultrasound apparatus is rapidly diversifying and has now developed from a static anatomical imaging technique to encompass the production of live, moving, images and measurement of a wide range of physiological functions.

The basic physical principles of diagnostic ultrasound apparatus are reviewed and recent advances in its clinical application presented. The latter include the use of high resolution ultrasound images to detect fetal abnormalities. Over 65 separate congenital anatomical abnormalities of the fetus have now been identified by ultrasound and many centres throughout the world have initiated routine screening programmes for the identification of unsuspected fetal anomalies. The recent improvement in image resolution and tissue differentiation has also permitted extension of ultrasound imaging to include many of the intra-abdominal organs. The progress in this field is best exemplified by reference to the localisation of the pancreas by virtue of its vascular anatomical relations. This organ can now be visualised almost routinely and recent technical developments permit us to identify not only the gland but also the duct system within it by an entirely non-invasive transcutaneous technique.

An additional recent technical development is the identification of Doppler-shifted frequency in the echoes returning from pulsed ultrasound systems. This facility has enabled the development of non-invasive vascular imaging systems which have recently been developed for the transcutaneous measurement of volume blood flow in accessible vessels.

The value of ultrasound in the field of fetal, pancreatic and vascular imaging was discussed and illustrated with selected clinical images.

45. The evaluation of risk to the patient. By E. E. POCHIN (introduced by A. J. PALFREY). *National Radiological Production Board, Chilton, Oxfordshire*

The risks of exposure to high doses of ionizing radiation were recognized within a few years of the discovery and first uses of X-rays and of radioactive materials. Extensive radiobiological investigations in the subsequent eighty years have indicated that some risks of later malignant or hereditary effects are likely to follow even the lowest doses, without any threshold effect. The approximate magnitudes of these risks have been assessed in a substantial number of prolonged epidemiological studies following known radiation exposure of the body or of individual organs at moderate dose; and adequate inferences can be made of the size of the risks to be expected from the low doses likely in diagnostic X-ray or radionuclide examinations.

No investigations of any comparable scope or duration have been made on possible late effects of ultrasound or nuclear magnetic resonance procedures. No indications have, however, been obtained that either early or late harm is likely to result from the exposures at the levels needed in such tests. It is, on the other hand, clearly impossible yet to be sure that there might not be fatal risks as low as those in the order of 10^{-5} which may apply to typical radiological examinations.

No extensive study appears to have been made of risks involved in imaging by endoscopic methods but it seems unlikely that any risk of fatality would approach the value of 2×10^{-4} that has followed needle biopsy of the liver in two large series.

The risks of different radionuclide and other radiological examinations can be tentatively assessed in terms of the absorbed doses of radiation received by the various organs or tissues, and the epidemiological evidence of the size of the risks applicable to each. Conventional diagnostic procedures appear, on this basis, to imply fatal radiation risks of from 10^{-6} to 10^{-4} for X-rays, and of 10^{-7} for radionuclide studies.

DEMONSTRATIONS

D.1. The epithelial–connective tissue junction in mucosae from different intra-oral sites: comparative morphometric studies of attachment mechanisms. By ELIZABETH BALE and F. H. WHITE. *Department of Human Biology and Anatomy, University of Sheffield*

Stratified squamous epithelia are attached to the adjacent connective tissue by a specialised basal lamina complex. This comprises localised zones of attachment on the basal plasma membrane, the hemidesmosomes, and a lamina densa, which forms a thin sheet in the connective tissue immediately below the epithelial basal plasma membrane. It has been suggested that the topography of the interface between these tissues is important in modifying the attachment, with areas under high stress possessing a more irregular, rete-ridge type configuration. The purpose of this report is to clarify the morphological nature of the epithelial–connective tissue attachment by comparing palatal and buccal mucosae in which the interfaces are convoluted and relatively flat, respectively.

Mucosal samples were obtained from five male ferrets from both cheek and hard palate. Tissue blocks were routinely processed for electron microscopy and flat-embedded in Araldite; semithin sections were prepared and stained with toluidine blue. This material was used to obtain an index of the degree of irregularity of the epithelial–connective tissue junction by measuring the lengths of the granular cell/keratin (L_{GK}) and epithelial–connective tissue (L_{EC}) junctions using a MOP (Kontron) semi-automatic image analysing system. The ratio of L_{EC}/L_{GK} provided such an index. From ultrathin sections obtained from the same blocks, a strict sampling procedure was used to acquire micrographs which included epithelial–connective tissue junction, at a final magnification of $\times 12100$. Using stereological intersection counting, the following parameters were estimated: the relative surfaces of hemidesmosomes to basal plasma membrane ($S_{Shd,\,bpm}$); the mean hemidesmosomal diameter (Δ_{hd}); and the number of hemidesmosomes per unit surface of basal plasma membrane ($N_{Shd,\,bpm}$).

Results suggest that in palatal mucosa, with a prominent rete-ridge pattern, values for $S_{Shd,\,bpm}$ and Δ_{hd} were substantially increased when compared with cheek mucosa, whereas $N_{Shd,\,bpm}$ values were similar in both tissues. Since mucosae from both sites have a similar hemidesmosomal frequency, it appears that palatal tissue which is subjected to higher stress possesses larger hemidesmosomes, resulting in an increase in $S_{Shd,\,bpm}$ thus providing a greater specialised surface for adhesion between the epithelium and underlying lamina propria.

D.2. Some morphometric aspects of epidermal carcinogenesis. By BUSHRA AL-AZZAWI and F. H. WHITE. *Department of Human Biology and Anatomy, University of Sheffield*

The histopathological diagnosis of malignant lesions of the oral mucosa is usually relatively straightforward, but this is not the case for pre-malignant lesions. Since the early detection of malignancy is accompanied by greatly improved survival, there is a requirement for assisting diagnosis, which is normally performed by predominantly subjective methods. The aim of the present report is to evaluate the application of objective histological methods to tissues subjected to chemical carcinogenesis which are known to be, or to become, malignant, with the long term view of improving the diagnosis of pre-malignant lesions. The parameters selected for evaluation are ones which can be detected readily on routine histological material.

The dorsal skin of 15 male Syrian golden hamsters was shaved and a 0·5 % solution of 7,12-dimethylbenz(α) anthracene (DMBA) was applied three times per week for periods up to 7 weeks. Samples of skin were removed at 9, 12 and 16 weeks after commencement of DMBA application from five animals at each interval. Five untreated animals served as controls. Using a semi-automatic image analysing system, the following parameters were estimated for each group: epidermal thickness (T), and the ratios epidermis/dermis (EP/DERM), epidermis/hypodermis (EP/HYP) and dermis/hypodermis (DERM/HYP).

Our results suggest that epidermal carcinogenesis is accompanied by increases in T, EP/DERM and DERM/HYP whereas the parameter DERM/HYP decreases at 9 weeks but returns to normal values by 12 weeks. These observations implicate previously undescribed volumetric alterations in the connective tissues. Since by far the majority of reports on experimental and human skin cancer are concerned with epithelial changes, our results lead us to suggest that the quantitative evaluation of the connective tissues might be beneficial in improving our understanding of the pathogenesis of these lesions. The specificity of these changes will require further investigation before they can be implicated as indicators of malignant change.

D.3. Volumetric alterations in the collagen content of the lamina propria during experimental oral carcinogenesis. By S. G. TARPEY and F. H. WHITE. *Department of Human Biology and Anatomy, University of Sheffield*

A variety of morphological changes accompanying the development of cancer in epithelial tissues has been reported. Studies on cancer development in epithelia have suggested that alterations in the collagenous component of the underlying dermis or lamina propria may facilitate the invasion of cancer cells. The aim of the present report is to quantify the volume of collagen fibres within the lamina propria of normal hamster cheek pouch mucosa. These data are compared with similar data obtained from similar sites during defined stages of carcinogenesis induced by the potent carcinogen, 7,12-dimethylbenz(α)anthracene (DMBA). In addition, we have introduced a non-malignant inflammatory control to assess the specificity of any alterations.

A 0·5 % solution of DMBA was applied to hamster cheek pouches. Tissue samples which could be diagnosed histopathologically as hyperplasia, dysplasia and carcinoma were obtained from five animals for each stage. Five untreated animals were used as normal controls. The inflammatory control was induced by a single topical sensitizing application of 5 % dinitrochlorobenzene (DNCB) in acetone to the dorsal skin of five animals followed by secondary topical application to the cheek pouches 10 days later. This procedure induced a delayed hypersensitivity reaction in the lamina propria of the pouches.

All tissue was immersed in a glutaraldehyde/formaldehyde fixative for 2 hours and routinely processed for electron microscopy. Following a strict sampling regime, electron micrographs were recorded from the epithelial–connective tissue junction at a final magnification of × 37500. Using stereological point counting, the volume density of collagen per unit volume of extracellular lamina propria was determined from the prints.

Our results describe a progressive decrease in the volume density of collagen during chemical carcinogenesis. The values obtained were 0·82, 0·54, 0·45 and 0·15 for normal, hyperplasia, dysplasia and carcinoma stages respectively. However, data for the inflammatory control provided a value of 0·43 which is similar to the dysplasia stage. These changes may reflect fundamental alterations in the lamina propria, and the extensive reduction in the collagenous component may provide a less restrictive environment through which invading cancer cells may pass. The results of our inflammatory control lead us to conclude that the loss of collagen in carcinomas may not be entirely the result of the inflammatory infiltrate which invariably accompanies such lesions.

D.4. The *in vitro* effects of histamine dihydrochloride on the sub-epithelial nerves of the rat ureter. By PAULINE BARBER and A. D. HOYES. *Department of Anatomy, St Mary's Hospital Medical School, London*

It has been suggested that histamine is a chemical mediator for cutaneous pain. There is evidence that the axons in the sub-epithelial nerves of the rat ureter are pain afferents. Two studies were undertaken to assess the effects of histamine on these axons in adult male Wistar rats. In the first study, specimens of ureter from each of six rats incubated *in vitro* in oxygenated Krebs Ringer bicarbonate buffer were exposed for 2 minutes to histamine at concentrations of 10^{-3}, 10^{-5}, 10^{-7} and 10^{-9} g/ml. One specimen from each rat was incubated in buffer alone and was used as a control. The specimens were then fixed with glutaraldehyde. In the second study, specimens from each of six rats were exposed *in vitro* to histamine at a final concentration of 10^{-3} g/ml for ½, 1, 2, 5 and 10 minutes before fixation in glutaraldehyde. A control specimen incubated in buffer alone was also processed from each rat. Electron micrographs were taken from sections of two blocks from each specimen. Measurements of axon and vesicle diameter and counts of the no./100 axon profiles of clear and large dense-cored vesicles were made on prints of the micrographs. No increase in either axon diameter or vesicle size or the number of vesicles per 100 axons was found, either after incubation in different concentrations of histamine or incubation for different times in the same concentration of histamine. These results suggest that histamine does not stimulate pain afferents. Further studies are now being undertaken to determine whether it has a sensitising effect on these axons.

D.5. Vasoactive intestinal polypeptide (VIP)-like immunoreactivity in the mammalian ureter. By A. D. HOYES, K. L. SIKRI, PAULINE BARBER and H. JAGESSAR. *Department of Anatomy, St Mary's Hospital Medical School, London* (Fig. 13)

VIP-like immunoreactivity has recently been demonstrated by immunofluorescence and gold-labelled antibody techniques in the intramural nerves of the cat and the guinea-pig ureter (Wharton *et al. Neuroscience* **6**, 1981). To provide further evidence on the distribution of VIP-like immunoreactivity in the ureter of these species, light and electron microscopical studies were undertaken on material processed by the peroxidase-antiperoxidase antibody technique. Specimens of ureter were fixed in periodate-lysine-paraformaldehyde. Those from the cat were fixed by immersion and those from the guinea-pig were fixed by vascular perfusion. Cryostat sections were treated with VIP antibodies and peroxidase-antiperoxidase complex, stained with diaminobenzidine and processed for electron microscopy.

Light microscopical studies were undertaken on cryostat sections and on sections 1 μm thick of material embedded in resin. In the cat, there were considerable amounts of immunoreactivity in nerves in the muscle coat (Fig. 13A, *m*) and in nerves associated with arterioles (Fig. 13A, *a*). There were also small amounts of immunoreactivity in nerves in the submucous and sub-epithelial connective tissue (Fig. 13A, *s*). In the guinea-pig, there were similar amounts of immunoreactivity in nerves in the submucosa and beneath the epithelium, but there was less reaction in nerves in the muscle coat (Fig. 13B, *m*) and in nerves related to blood vessels. In ultrathin sections, reaction product was seen in only a proportion of the axons in the nerves. In both the cat (Fig. 13C) and the guinea-pig (Fig. 13D), it was present in axon terminals containing mainly small vesicles. Large vesicles containing reaction product were only occasionally seen in these terminals, and the immunoreactivity was located mainly on the membranes of the small vesicles (Fig. 13C, D). There was no evidence of reaction product in terminals containing mainly large vesicles.

The findings of the present study differed from those reported by Wharton *et al.* (1981) in that, in the guinea-pig, there were larger amounts of immunoreactivity in the plexuses and that, at the ultrastructural level, there was evidence of reaction product only in axons with terminals containing mainly small vesicles. These differences may be due to technical factors, and in particular to the use of different fixation and immunocytochemical procedures to those employed by these authors.

We are indebted to Dr J. M. Polak for the supply of VIP antibodies used in this study and to the Wellcome Trust for financial support.

D.6. Collagen Type I in the early chick embryo. By MARJORIE A. ENGLAND, D. R. CRITCHLEY* and G. SHELLSWELL†. *Departments of Anatomy and *Biochemistry, University of Leicester and † Agriculture Research Council, Meat Research Institute, Nr. Langford, Bristol* (Fig. 14)

An arc of extracellular fibres has been described on the anterior area pellucida/area opaca border of the gastrulating chick embryo. This fibrous band is present on the ventral surface of the ectoblast. It is exposed by fixing the chick embryo in 4% formalin in phosphate-buffered saline (PBS)/or Karnovsky's fluid and subsequently dissecting off the endoblast and mesoblast layers. This leaves the ventral ectoblast exposed for examination. In the present study the stage 4 chick embryo was examined by scanning electron microscopy as a control and by immunochemistry. It was previously reported that this arc of fibres stained prominently for the presence of fibronectin in a concentration of 1:25 using PBS. This was also used as a control for the present study. The present communication reports the findings of staining with anti-chick collagen Type I.

The fibrous band stains prominently with anti-collagen I (Fig. 14A) as does the expanding edge of the blastoderm in contact with the vitelline membrane (Fig. 14B). The fibres in the band are prominently stained, while the expanding edge cells are outlined.

These findings further clarify the composition of the fibrous band. As this band is functionally of importance in normal morphogenetic movements in the embryo and in primordial germ cell migration its composition is relevant.

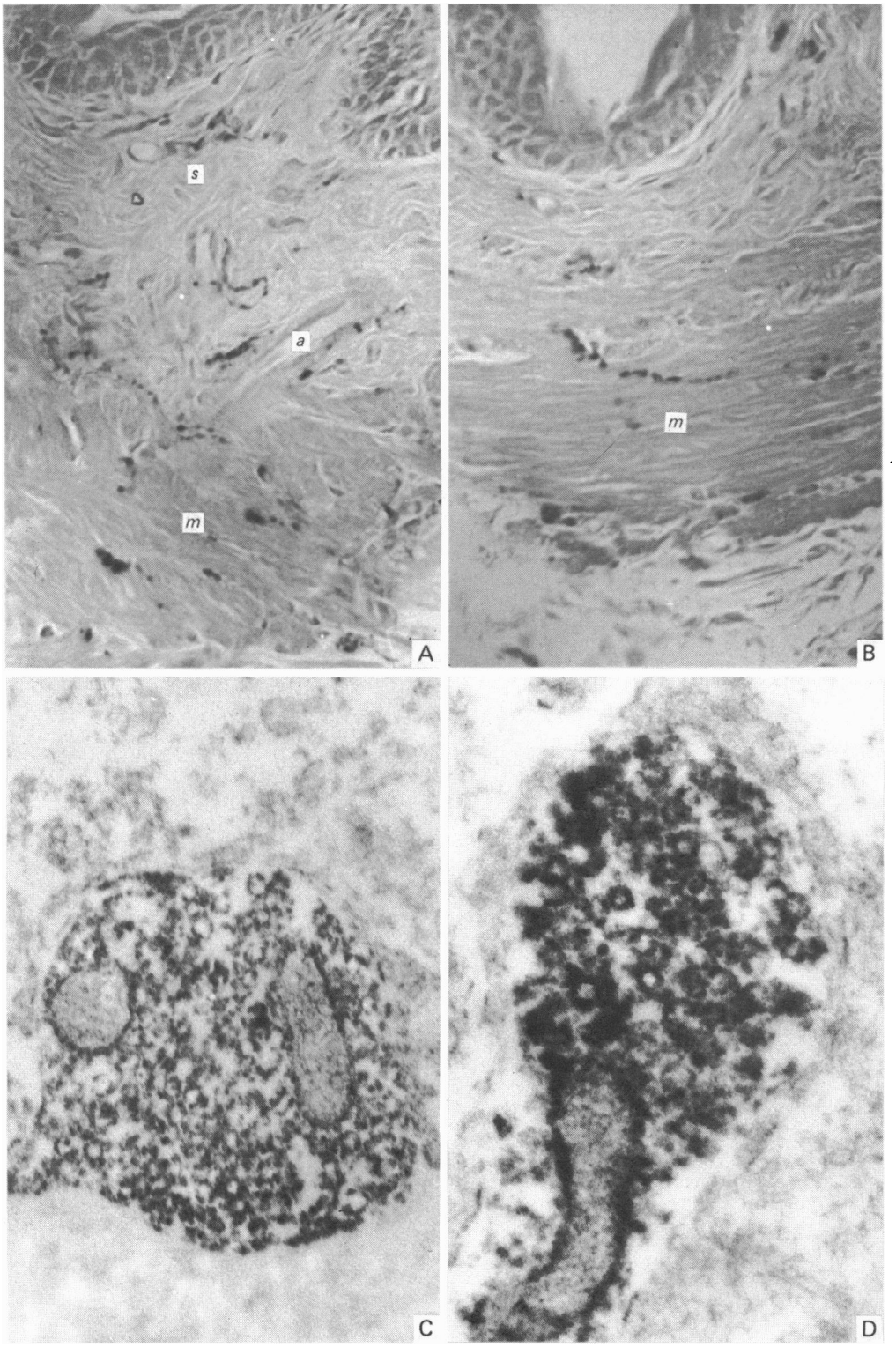

Fig. 13.

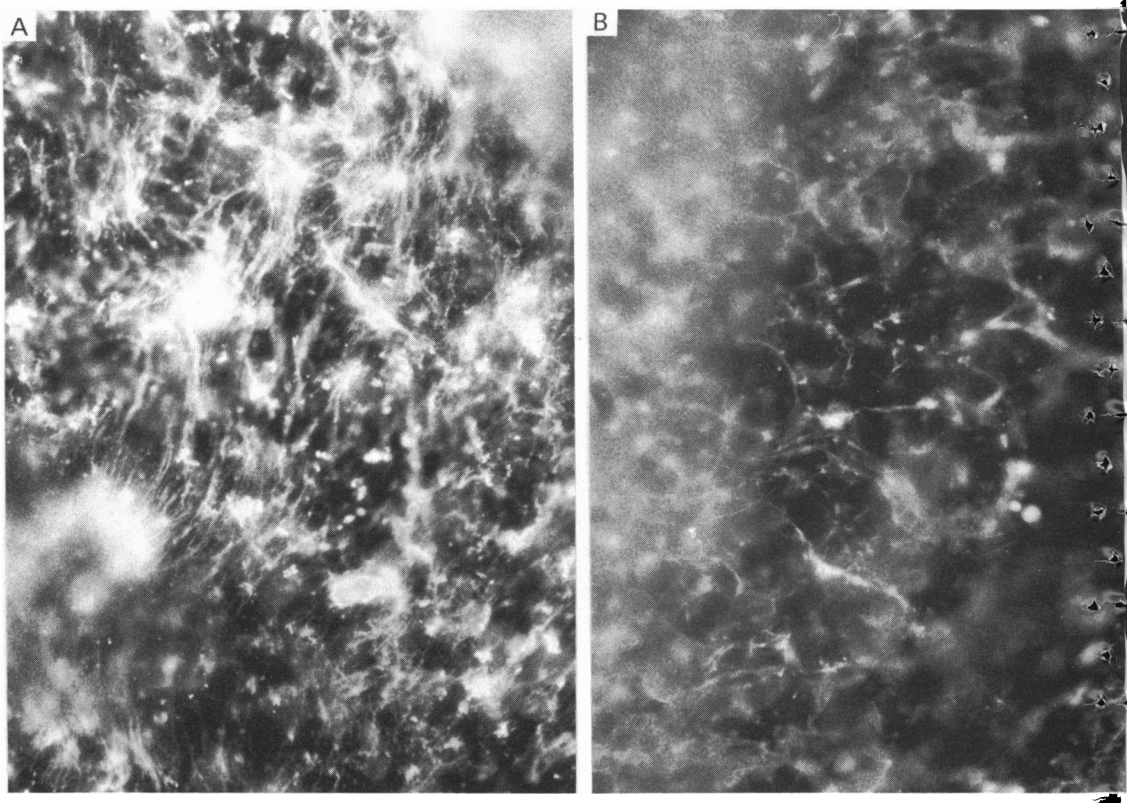

Fig. 14

D.7. Extracellular materials in the early quail embryo. By MARJORIE A. ENGLAND and CAROLE PERCIVAL. *Department of Anatomy, University of Leicester* (Fig. 15)

Patterns of extracellular materials which alter during gastrulation have been described in the early chick embryo. In the present study the gastrulating quail embryo has been examined by scanning electron microscopy to determine if the same patterns occur. Stage 4 embryos were fixed in a mixture of aldehydes and subsequently the mesoblast and endoblast layers were dissected off exposing the ventral surface of the ectoblast for examination.

The same three patterns of extracellular materials present in the chick embryo are also present on the quail ventral ectoblast layer. On the anterior area pellucida/area opaca border is an arc of several fibres. The fibres are similar in appearance to those found in the chick embryo (Fig. 15A), but they form a wider band in the quail. Fibres are present radiating from the primitive streak region but are shorter in length and not as numerous as those found in the gastrulating chick. A small area of vertically orientated rods of extracellular materials is present immediately in front of the arc of fibres in the direction of the primitive node, but is much smaller than that found in the chick.

The three patterns of extracellular materials in the quail are similar to those described in the chick embryo but differ in degree and quantity.

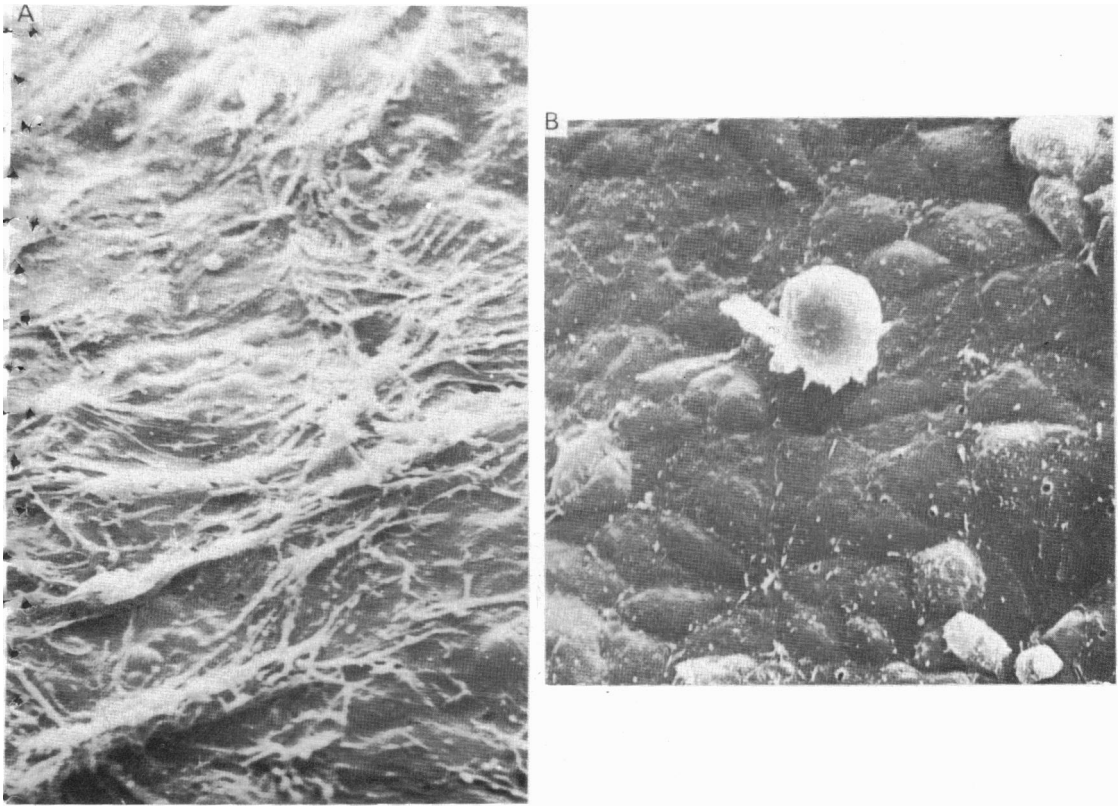

Fig. 15

D.8. Gastrulating chick embryo primordial germ cells in an ectopic site. By MARJORIE A. ENGLAND. *Department of Anatomy, University of Leicester* (Fig. 15)

Chick embryo primordial germ cells (PGC) are present in the endoblast and subsequently separate from this layer and migrate caudally between the ectoblast and endoblast. This active migration is contrary to other morphogenetic movements in the gastrulating embryo. In the present study the PGC were observed on the outer surface of the endoblast.

Stage 4 chick embryos were fixed in Karnovsky's fluid and subsequently prepared for scanning electron microscopy. The PGCs were located in the anterior half of the embryo in the area pellucida. Their morphological appearance was similar to their normal appearance when located between the ectoblast and endoblast. Cells were rounded with long pseudopodial extensions with ruffled membranes at their tips (Fig. 15B). Several cells were located in naturally occurring spaces in the endoblast where new cells are normally added to the endoblast layer.

The finding of PGCs on the outer surface of the endoblast suggests that they are invasive by nature, and that several do not reach their normal caudal destination but migrate in ectopic sites.

D.9. Some numerical characteristics of the discrete helical axes determined in a roentgen-photogrammetric analysis of tarsal movements. By E. J. VAN LANGELAAN (introduced by A. HUSON). *Department of Anatomy and Embryology, University of Leiden, The Netherlands* (Fig. 16)

We reported in earlier communications on the method and some preliminary results of a roentgenphotogrammetric analysis of the supinatory tarsal movements following tibial lateral rotation (*J. Anat.* **117**, 1974; **126**, 1978). Since that time data from experiments in 10 more leg specimens have become available, and these are presented.

In each specimen we calculated from six positions of the tibia and the tarsal bones five discrete helical axes as approximations of the instantaneous axis of motion. The position of these axes is characterised by a deviation angle π (angle between axis and sagittal plane) and an inclination angle ϕ (angle between axis and horizontal plane). In each of the ten specimens we determined the mean value of π and ϕ for five positions. They are presented as absolute axes (ABS) for the movements of each separate bone, and as relative axes (REL) for the intertarsal movements. The range of values is as follows:

(*a*) Abs TIBIA	π max. 78·8°	π min. 4·3°	ϕ max. 87·6°	ϕ min. 82·9°
(*b*) Abs TALUS	π max. 76·5°	π min. 45·1°	ϕ max. 86·7°	ϕ min. 55·8°
(*c*) Abs CALCANEUS	π max. 22·7°	π min. 4·0°	ϕ max. 60·0°	ϕ min. 25·6°
(*d*) Abs NAVICULAR	π max. 23·9°	π min. 2·6°	ϕ max. 17·9°	ϕ min. 5·0°
(*e*) Abs CUBOID	π max. 15·2°	π min. 2·5°	ϕ max. 16·7°	ϕ min. 3·0°
(*f*) Rel TACA	π max. 40·3°	π min. 8·4°	ϕ max. 54·2°	ϕ min. 23·2°
(*g*) Rel CUCA	π max. 33·6°	π min. 3·4°	ϕ max. 72·1°	ϕ min. 43·2°
(*h*) Rel TANA	π max. 23·7°	π min. 4·2°	ϕ max. 49·6°	ϕ min. 24·3°

The angle between two successive discrete axes is called γ. These angles γ have been summed ($\Sigma\gamma$). The range of values is given below:

(1) Rel TACA	$\Sigma\gamma$ max. 88·9°	$\Sigma\gamma$ min. 10·1°
(2) Rel CUCA	$\Sigma\gamma$ max. 58·4°	$\Sigma\gamma$ min. 10·0°
(3) Rel TANA	$\Sigma\gamma$ max. 32·9°	$\Sigma\gamma$ min. 13·1°

In the demonstration we also present the paths of six intersection points of the helical axes with a chosen plane and the 3-D projection of the successive axes. Fig. 16 is an example of the relative talocalcaneal (subtalar) movement. Note the oblique axis, moving in the course of supination in a posteromedial direction along the canalis tarsi.

A summary of the rotations around and translations along these helical axes is presented.

D.10. Cellular and nuclear volume changes during the development of experimental oral cancer. By F. H. WHITE, R. M. CODD and K. GOHARI. *Departments of Oral Pathology, and Human Biology and Anatomy, University of Sheffield.*

One of the characteristic cytological features of squamous cell carcinoma is the heterogeneity of the individual cell components. It has been suggested that cells within pre-malignant epithelia also demonstrate cellular and nuclear pleomorphism, and indeed these features are commonly used by histopathologists when making their assessment of the malignant potential of a particular lesion. We decided to evaluate the reliability of this alteration by estimating cellular and nuclear volumes in a controlled experimental carcinogenesis system.

Following application of 0·5 % 7,12-dimethylbenz(α)anthracene (DMBA) to cheek pouch mucosa, the epithelial lining passes through a series of histopathological pre-malignant stages which can be classified as hyperplasia and dysplasia, before becoming malignant. Mucosal specimens were obtained from five animals from each of these stages and five untreated animals served as controls. Using a systematic stratified sampling procedure, electron micrographs were obtained from defined basal, spinous and granular layers for each of normal and hyperplasia, dysplasia and carcinoma groups. Direct nuclear measurement was used to obtain estimates of mean nuclear diameters which were then converted to those of circles of equivalent area. These transformed diameters were then used to determine nuclear volumes (V_N) for each layer at each stage. Stereological point-counting procedures were used to determine the nuclear–cytoplasmic ratio (N/C) for all the layers and stages. By substituting V_N into N/C it was possible to derive

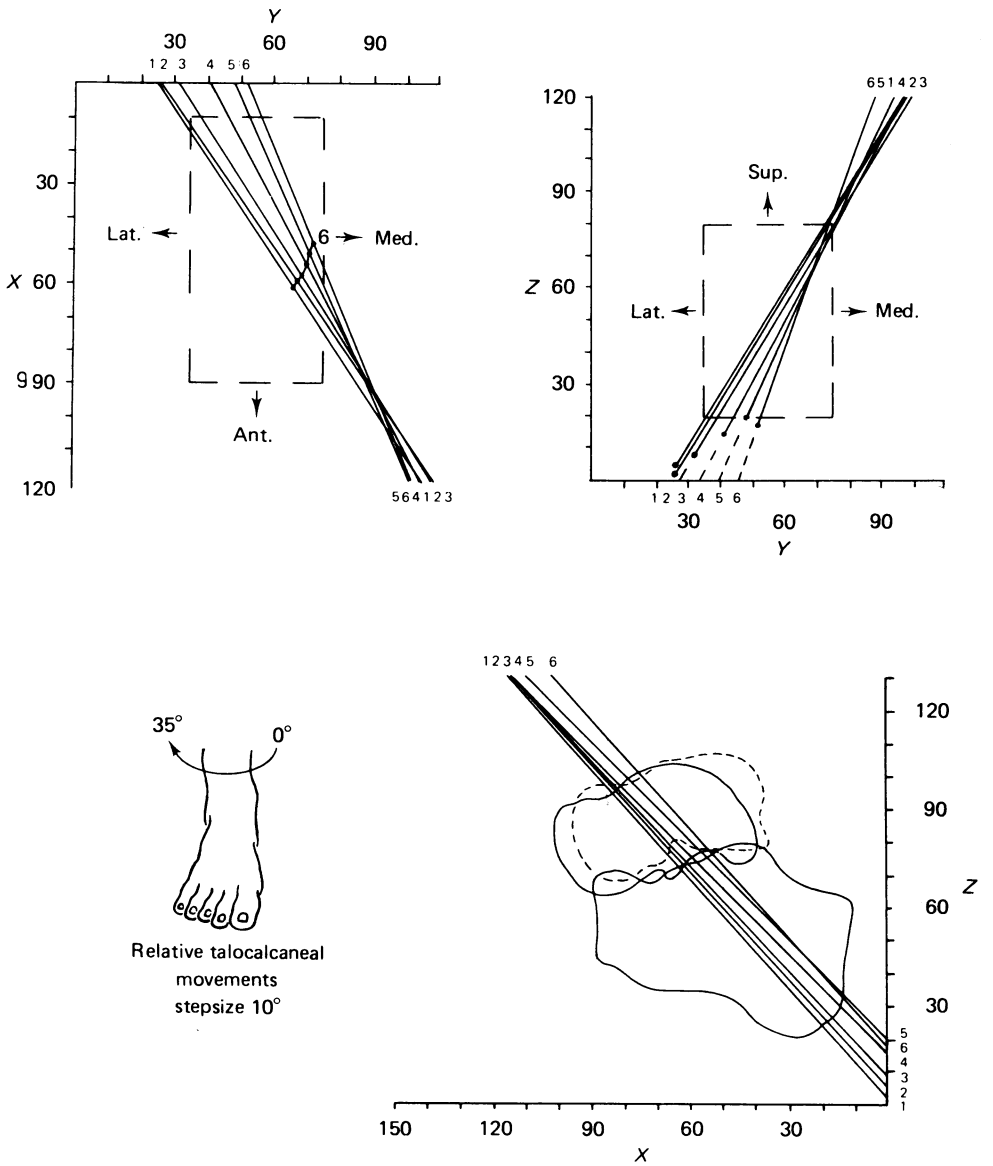

Fig. 16

an estimate for mean cytoplasmic volume (V_C) and then mean cell volume (V_{cell}). Values for V_N increased progressively during carcinogenesis in all cellular layers, with values being highest in the spinous layer. V_C increased to a greater extent than V_N; in carcinomas V_C was about three times greater than in normal tissue. From these results it appears that cancer development is accompanied by increases in cellular volume that are the consequence of differential increases in both cytoplasmic and nuclear volumes. The increases in standard deviations during carcinogenesis reflect the cellular pleomorphism of these lesions that is visible on histological examination.